Journal of Biochemical and Molecular Toxicology

WILEY

RESEARCH ARTICLE

Anticancer Activity of Fisetin via KEAP1, DNMT1, and mTOR Axis Against Colon Cancer: An Integrated In Silico, In Vitro, and In Vivo Approach

Satyam Sharma[1] | Rajat Mudgal[2] | Sairam Krishnamurthy[2] | Sanjiv Singh[1]

[1]Department of Pharmacology & Toxicology, National Institute of Pharmaceutical Education and Research, Hajipur, India | [2]Department of Pharmacology, Indian Institute of Technology-Banaras Hindu University, Varanasi, India

Correspondence: Sanjiv Singh (sanjivpg2006@yahoo.com; sanjivsingh@niperhajipur.ac.in)

Received: 26 March 2025 | **Revised:** 6 June 2025 | **Accepted:** 24 June 2025

Funding: This work was supported by the Department of Pharmaceuticals, Ministry of Chemicals and Fertilizers, Govt. of India.

Keywords: angiogenesis | colon cancer | DNMT1 | fisetin | KEAP1 | Ki67 | mTOR

ABSTRACT

The proliferation of colon cancer is influenced by alterations in epigenetic, reactive oxygen species (ROS), and dysregulation of signaling pathways, especially via the involvement of DNMT1, mTOR, and KEAP1 axis. The current investigation examined the antiproliferative capabilities of fisetin (FisT) in a rat model and in colon cancer cell lines HCT116, CT-26, and Caco-2. Our findings show that FisT modulated the DNMT1, mTOR, KEAP1, and IL-6 signaling pathways to enhance the antiproliferative effects against in vitro and in vivo preclinical model. In-silico based anticancer potential of fisetin were revealed through SwissTargetPrediction, Cytoscape, STRING, Schrodinger, molecular dynamics simulations, KEGG, and network analysis. In-vitro MTT assay, cell cycle analysis, ROS level, immunocytofluorescence, western blot analysis, and in vivo immunohistofluorescence, western blot analysis, ELISA-based assays were performed to evaluate anticancer property of fisetin. Our findings revealed that FisT has a strong anticancer property by demethylating DNA, enhancing ROS, KEAP1 level. Simultaneously downregulated the DNMT1 & mTOR expression, and preventing angiogenesis, cell proliferation, invasion, and migration against in vitro & in vivo models. FisT enhances the anticancer response of tumor development and reduces the size of crypt foci. FisT has potential as a cytotoxic drug, improving and intensifying anticancer responses in colon cancer.

1 | Introduction

Colon cancer is the 3rd most common disease worldwide, and more than 1.2 million new cases arise every year and cause 600,000 deaths annually [1]. Mounting evidence has indicated that upregulation of DNMT1, m-Tor, and downregulation of Keap-1 level leads detrimental effect on colon cancer patients, including enhancing angiogenesis, metastasis, worsening quality of life, increased cancer risk as well as shortened survival rates [2, 3]. Thus, aggressive identification and treatment of colon cancer patients is critical. At present, First-line treatments for colon cancer, including chemotherapeutic agents such as 5-fluorouracil (5-FU), capecitabine, and oxaliplatin, and targeted therapies like bevacizumab and cetuximab, often face limitations due to resistance, target pathways redundancy, toxicity, and therapy-associated mortality. These challenges highlight the potential utilizations of phytomolecules, with their multi-targeted mechanisms, low toxicity, and ability to modulate critical cancer pathways, as promising alternatives or adjuncts to conventional therapies. Therefore, it is essential that we develop a nontoxic therapy having therapeutic effects on colon cancer [4–7].

Flavonoids, composed of a 15-carbon skeleton arranged in a C6−C3−C6 configuration, are naturally occurring polyphenolic compounds with diverse biological properties [8]. Flavonoids interfere with critical signaling pathways involved in cancer development which leads to potent anticancer action with limited toxic effects [9]. Medicinal products as well as their active constituents, especially flavonoids produced from various plants, can effectively decrease proliferation of tumors, induce apoptosis, and decline chemotherapy resistance in colon cancer [10].

FisT, a naturally produced flavonoid found to prohibit cell proliferation, induces apoptosis, modulates signaling pathways (PI3K/Akt, MAPK, and NF-κB), and suppresses angiogenesis [11, 12]. The capability to target various biological pathways has made it an attractive option for chemotherapy for colon cancer, with possible benefits in reducing tumor growth, metastasis, and drug resistance [13]. Several previous research findings suggesting that FisT can effectively inhibit the cell proliferation, migration, and metastasis of colon cancer cells by upregulating the expression levels of Keap-1 and downregulating the DNMT-1 and mTOR. In particular, it was found that DNMT-1 was overexpressed in MCF-7 & MDA-MB-231 cell lines treated with FisT were downregulated the expression level and shown anticancer response [12, 14–18]. Accordingly, FisT might alter a number of mechanisms and targets to exhibit anticancer effects.

Fisetin, a flavonoid from natural origin, has shown to have anticancer effects against colorectal cancer (CRC) models, such as induction of apoptosis and inhibition of proliferation via various pathways such as PI3K/Akt/mTOR and Wnt/EGFR/NF-κB [12, 19]. Nevertheless, its direct effect on the interacting KEAP1/DNMT-1/mTOR axis is not yet sufficiently explored. KEAP1 dysfunction in CRC induces persistent activation of Nrf2 by inhibiting its degradation. This results in elevated expression of antioxidant and detoxifying enzymes, metabolic reprogramming that neutralizes chemotherapy-induced reactive oxygen species (ROS), and augmented drug resistance against conventional treatments such as 5-FU and oxaliplatin. Nrf2 further upregulates multidrug resistance transporters and anti-apoptotic proteins, and induces EMT (epithelial−mesenchymal transition) by SNAIL and TWIST1, allowing metastasis [19, 20]. KEAP1 aberration in CRC leads to Nrf2 activation, which increases antioxidant defenses and drug resistance. Simultaneously, DNMT1, an epigenetic modifier that is mostly overexpressed in CRC, hypermethylates and silences tumor suppressor genes, facilitating cancer growth. This epigenetic silencing, together with Nrf2-mediated metabolic reprogramming and expression of drug resistance proteins, facilitates tumor survival, therapy resistance, and metastasis. Recent evidence indicates that inhibition of the KEAP1-Nrf2 axis in combination with DNMT1-induced epigenetic alterations provides a promising therapeutic strategy in CRC [21–23].

The mTOR pathway, frequently hyperactivated in CRC, is responsible for tumor growth, survival, and metabolic reprogramming. Its activation is in close association with the KEAP1 and DNMT1 status, with KEAP1 dysfunction inducing Nrf2 antioxidant signaling and DNMT1 overexpression inducing epigenetic silencing of tumor suppressors. The synergism of these alterations enhances the mTOR signaling, driving cancer advancement, therapy resistance, and metastasis. Targeting this interconnected axis has potential to enhance the outcome of treatment in CRC [24]. While fisetin has been shown to inhibit mTOR signaling in prostate cancer cells [25]. Its effect on mTOR activity in CRC, particularly in the context of KEAP1, DNMT1, and m-TOR involvement, together is not well-defined.

In spite of increasing evidence of fisetin's anticancer activity against CRC, its specific molecular targets remain poorly characterized. Most importantly, the mutually interconnected KEAP1/DNMT1/mTOR axis that plays a pivotal role in maintaining redox homeostasis, epigenetic silencing, and oncogenic signaling has not been mechanistically investigated in the context of fisetin treatment. KEAP1 loss results in constitutive Nrf2 activation [26], DNMT1 hyperactivity epigenetically silences tumor suppressors [27], and mTOR supports survival and chemoresistance [28]. Whether fisetin has the capacity to modulate this axis to reverse therapy resistance and suppress CRC development is yet to be explored. This deficiency hampers its complete potential in therapy. Research into fisetin's regulatory effect on KEAP1/Nrf2, DNMT1, and mTOR may uncover a new tri-targeted mechanism to advance fisetin from a broad antioxidant to a pathway-specific epigenetic and redox modulator in CRC treatment [29, 30].

The current investigation established a network of FisT-target protein signaling pathways using network pharmacology analysis and the docking approach. Identifying FisT targets and related pathways to further investigate its anticancer capabilities in a preclinical anticancer model. The anticancer activity of FisT was evaluated by performing the immunoassays for target proteins, ROS level, Hoechst staining, H2DCFDA staining, Keap-1, DNMT1, and mTOR expression level by advanced sophisticated techniques such as: Immunocytochemistry, immunohistochemistry (IHC), western blot (WB) analysis, FACS, ELISA, histological assessments, and so forth against Caco-2 cell lines and DMH induced CRC model in wistar rats. At the end of this study, we will be able to find out novel approaches to treat colon cancer by avoiding pathways redundancy and therapy resistance in cancer cells and colon cancer patients with Keap-1, DNMT1, and mTOR alterations.

2 | Materials and Methodologies

2.1 | In-Silico Studies

2.1.1 | FisT Target for Combating Colon Cancer by Network Pharmacology

Potential targets for colon cancer were gathered from databases such as Gene Cards, CTD, and Geodis Net, whereas FisT targets were found via the Gene Cards platform. Venn diagram analysis was used to identify overlapping targets and highlight common therapy targets. Using the STITCH database, a compound-target interaction network for FisT was created and shown, with FisT serving as the center node and connecting to its targets. A protei−protein interaction (PPI) network was created using the STRING database and examined in Cytoscape to determine

the degree of interaction between nodes. SHINYGO was used to undertake Gene Ontology (GO) and KEGG pathway enrichment studies, which identified enriched biological processes, molecular functions, cellular components, and KEGG pathways, with findings sorted by fold enrichment and corrected *p*-values.

2.1.2 | Protein–Ligand Preparation and Grid Generation

PDBQT data were taken from substantially optimized DNMT-1, Keap-1, and MTOR proteins PDB databases (3AV5) using Auto Dock tools 1.5.6. Using energy reduction utilizing the MMFF94 field of force in Chem3D, the ligand FisT structure was obtained through PubChem and saved as a PDB file. The Auto Dock 1.5.6 tools' ligands preparations component was implemented to convert the PDB into PDBQT. To determine the interaction energies of various atoms in the ligand, grid maps were computed using 8 Auto grids 4.0 [31, 32].

2.1.3 | DNMT1-KEAP1-mTOR Docking

The structure of DNMT1 (351–1600) with PDB ID 3AV5 was determined using X-Ray diffraction at a resolution of 2.66 Å. The SAH was bound to the DNMT1 binding pocket in the MTase region, which contained 28 residues: Asp1146, Val1147, Phe1148, Ser1149, Gly1150, Cys1151, Gly1152, Gly1153, Leu1154, Ser1155, Ile1170, Glu1171, Met1172, Trp1173, Ala1176, Glu1192, Asp1193, Cys1194, Asn1195, Gly1225, Gly1226, Pro1228, Leu1250, Glu1269, Arg1576, Asn1580, Ala1581, Val1582. According to the obtained PDB structure, SAH was observed to form eight hydrogen bond interactions with GLU1171, MET1172, 1192 GLU, CYS1194, 1226GLY, and 1228 PRO, Phe1148, Gly1153, Leu1154, Glu1171, Asp1193, Cys1194, and 1148 PHE. Identifying the native substrate and binding site is a critical step in developing an effective inhibitor for a certain target protein of interest. The grid box size for covering active site areas of proteins is $54 \times 62 \times 74$, with a grid spacing of 0.375 Å and the grid center at 11.177, −7.564, and 38.121 for x, y, and z coordinates.

The mTOR crystal structure was retrieved from the Protein Data Bank (4JSV). The initial structure of 4JSV is a homodimer containing two identical complexes of the atypical kinase mTOR and the ligand mLST8. We eliminated one of the complexes and the ligand mLST8 to get the monomer structure of the MTOR-encoded receptor protein for further molecular docking. The grid box size for covering active site areas of proteins is $52 \times 68 \times 72$, with a grid spacing of 0.375 Å and the grid center at 12.177, −8.564, and 36.121 for x, y, and z coordinates.

The Keap-1 crystal structure was acquired from Protein Data Bank (4L7B), and we ran molecular docking simulations using AutoDock. All water molecules and ligands were removed from Keap1's original structure, and polar hydrogen atoms were added before docking. The grid box was cantered for each target at the native binding location. The grid box size was set to $16 \times 16 \times 16$ Å, with the center at positions $\times = -2.4$, $y = 2.8$, and $z = -29.21$.

2.1.4 | Molecular Dynamic Simulation (MDS)

Another computation biology-based simulation technique that is frequently employed to comprehend the behavior of biological biomolecules as a consequence of time as well as the conformational changes that occur in their specific environments is called MDS. DNMT1 with FisT complexes MD was performed out using the Gromacs 2020, Schrodinger 2015-1 tool at Department of Pharmaceutical Engineering & Research, Indian Institute of Technology (IIT-BHU-Varanasi). A hydrated cubic box with a TIP3P (Transferable Intermolecular Potential with 3 Points) was used for soaking the protein–ligand combination. A total of 12 inches was selected as the cut-off measurement. Before the MD run, the system underwent a number of processes, including energy reduction, heating, as well as density equilibrium. As an NPT ensemble, the timing was set for 100 ns at 314.15 K of temperature [33].

2.2 | Reagents and Cells

The HCT116 (Culture Conditions: McCoy's 5 A + FBS), Caco-2 (Culture Conditions: MEM [E] with NEAA + FBS) cell lines were obtained from an accredited National Center for Cell Science Complex, Savitribai Phule Pune University Campus, Ganesh hind Road, Pune, 411007, India, Maharashtra State India and CT26 (Culture Conditions: RPMI [E] with NEAA + FBS) procured from Department of nano pharmaceutics laboratories, Institute of Nanoscience and technology, INST-Mohali, India. Dulbecco's Modified Eagle's Medium (DMEM), RPMI (Roswell Park Memorial Institute 1640), and MEM (Minimum Essential Medium) were purchased from Thermofisher Scientific (Gibco; Cat. No: 11965092), supplemented with 10% fetal bovine serum (FBS) (Thermofisher Scientific: Gibco; Cat. No: 10099141) & antimicrobial agents, such as streptomycin and penicillin (Thermofisher Scientific: Gibco; Cat. No: 15140122), to avoid contamination. To promote the best possible development and viability, the cells were carefully kept in a regulated environment at 37°C with a humidified atmosphere and 5% carbon dioxide added. These cells were confirmed to be free of contamination from other human cells and mycoplasma. FisT (FT) and 5-FU were obtained from TCI Chemicals (India) Pvt. Ltd. (Division of Tokyo Chemical Industry). Methanol, DMSO, and phosphate-buffered saline (PBS) were sourced from Sigma-Aldrich India. To reduce the possibility of contamination and ensure the preciseness of the data, the experiments were carried out using the purest water possible, with a resistivity of 18.2 MΩ-cm, obtained from a double-stage water purifier (Elix 20/35/70/100 Water Purification System). All chemicals used were of analytical grade. DMEM was purchased from Invitrogen Thermo Fisher India, and 5-FU was sourced from TCI Chemicals India. Primary antibodies against MTOR, Keap-1, Ki67, DNMT-1, & secondary antibodies Alexa Fluor 488, 594, and HRP-conjugated secondary antibodies were purchased from Abcam India. Hoechst staining, h2dcfda, DAPI from (Sigma Aldrich India), RIPA protease inhibitors tablets were from (Sigma Aldrich India). All biochemical reagents and ELISA kits were obtained from Sigma-Aldrich India. Other reagents used in this study were also of analytical grade.

2.3 | In-Vitro Experimentations

The adherent cells have been divided into three groups: Group I (Control group) received 1% DMSO treatment; Group II received FisT treatment at IC50 value; and Group III received 5-FU treatment at IC50 value. The experiments were conducted in triplicate across three independent trials. At 70%−80% confluence, HCT116, CT26, as well as Caco-2 cells were exposed to all regimens. After 48 h of incubation in a CO_2 an incubator, the cells were first trypsinized and were prepared for in vitro molecular analyses right away. To use immunoassays to detect Keap-1, Ki67, DNMT-1, m-TOR, and various other markers, the supernatants were kept at −80°C.

2.3.1 | Cytotoxicity Evaluations by MTT Assay

The MTT test was used to evaluate FisT impact on cell viability. A 96-well plate containing 5×10^3 cells per well was used to seed HCT116, CT26, and Caco-2 cells. The cells were then treated for 48 h with different doses of FisT and 5-FU as a reference (Control, 2.5, 5, 10, 20, 40, 80, 160 μM and Control, 1.5, 3, 6, 12, 24 μM). Following treatment, cells underwent incubation for 4 h with 10 μL of MTT solution (0.5 mg/mL) after the media was withdrawn. After dissolving the resultant formazan crystals in 100 μL of DMSO, a Multimode SpectraMax Microplate Reader (Molecular Devices, LLC3860 N First Street, San Jose, CA 95134) was used to determine the optical density (OD) at 490 nm [34].

Cell viability was ascertained utilizing a standardized formula: Cell viability (%) = $(OD_{FisT} - OD_{blank})/(OD_{control} - OD_{blank}) \times 100\%$. The test was parallel conducted in triplicate.

2.3.2 | Clonogenicity Assessment Assay

The cell lines of Caco-2 were incubated for an entire day after being plated in 6 cm culture dishes (1×10^3 cells/dish). After that, they received a further 2 weeks of treatment with FisT (160 μM) and 5-FU, which (24 μM) alone ($n = 3$). Following treatment, the colonies were fixed by methanol further stained with crystal violet for 15 min, and then rinsed with PBS. The colonies were then washed gently, dried, and observed under a Zeiss microscope, image captured through Axiocam 208 color camera, image analysis scaling done on ZEN blue software version 3.4.91.0 (Zeiss Inc. Germany) at Department of Pharmacology & Toxicology, NIPER Hajipur India. The number of colonies was counted and analyzed using ImageJ 1.42 software [35].

2.3.3 | Cell Migration Assay

A cell migration experiment was used to evaluate the Caco-2 cells' ability to move. In six-well plates, Caco-2 cells (1×10^5 cells/mL) were incubated overnight. After meticulously scraping the cell monolayer using the tip of a yellow pipette, the wells were cleaned with DMEM to get rid of any remaining cell debris. Fresh medium containing FisT (160 μM), 5-FU (24 μM), was added to the respective wells and incubated for 48 h ($n = 6$). At 0 and 48 h, the wound area in each well was photographed using a Zeiss microscope, image captured through an Axiocam 208 color camera, image analysis scaling done on ZEN blue software version 3.4.91.0. (Zeiss Inc., Germany) at Department of Pharmacology & Toxicology, NIPER, Hajipur, India. Cell motility was determined by counting the number of cells that migrated into the wound area by ImageJ 1.42 software [36].

2.3.4 | Hoechst Staining Assay

Using sterilized cover glasses within six-well plates, colon cancer cells (Caco-2 Cells) up to 1×10^5 cells per well. After attachment, cells were incubated for 48 h in fresh media with FisT (Fist: 160; 5fu 24 μM). After treatment, the cells have been fixed, rinsed three times with PBS, and stained for 5 min at the ambient temperature in the dark using 0.5 mL of Hoechst 33258 staining solution (Sigma-Aldrich, India; Cat: 94403). After two PBS washes, the stained nuclei exhibiting apoptotic characteristics were classified and graded based on the chromatin's staining and DNA condensation properties, which were then examined under a fluorescence microscope. image captured through Axiocam 208 color camera, image analysis scaling done on Zeiss microscope, image captured through Axiocam 208 color camera, image analysis scaling done on ZEN blue software version 3.4.91.0. (Zeiss Inc., Germany) at Department of Pharmacology & Toxicology, NIPER, Hajipur, India. Ten random fields per dish were observed and counted [37].

2.3.5 | ROS Level by Flow Cytometry

We employed the ROS-sensitive probe 2',7'-dichlorodihydrofluorescein diacetate (2′,7′-Dichlorodihydrofluorescein diacetates [Cat. 4091-99-0]) to determine the intracellular ROS level. To create a 10 mM solution of stock, H2DCFDA had been dissolve into DMSO afterwards subsequently adjusted before utilized. After 30 min of dark incubation at 37°C with 5 μM staining solution in PBS, adherent cells (Caco-2) were collected using 0.05% trypsin EDTA solution, suspended in a new medium, and promptly examined using a flow cytometer (BD Life Sciences). Both control and FisT-treated cell lines were suspended in PBS, incubated for 30 min at 37°C in the dark with 5 μM of H2DCFDA, and then promptly analyzed. Sample processed using a Flow Cytometer (BD FACS Aria Fusion, India). The data were processed and analyzed using BD FACS Diva 9.0.1 software [38].

2.3.6 | ROS by Fluorescent Microscopy

The oxidized H2DCFDA fluorescence in Caco-2 cells was observed simultaneously by growing the cells on cover slips after FisT treatment, followed by H2DCFDA treatment & investigation. For 60 min at 37°C in the dark, coverslips containing cells were submerged in a 5 μM H2DCFDA staining solution in PBS. Afterwards, they were cleaned and examined using a Zeiss fluorescent microscope using an Axiocam 208 color camera and ZEN 3.9 software on FITC channel. ImageJ

software (US National Institutes of Health) was used to quantify the signals. To put it briefly, each cell's cell membrane has an area of interest (ROI) that was manually marked along it. The average fluorescence intensity per cell unit area is then calculated [38] (shown as DCF/area), and the average integrated fluorescence density obtained from a single cell (represented as DCF/cell) were examined inside the ROI. Image were observed under a Zeiss microscope, image captured through Axiocam 208 color camera, image analysis scaling done on ZEN blue software version 3.4.91.0 (Zeiss Inc., Germany) at Department of Pharmacology & Toxicology, NIPER, Hajipur, India. Ten random fields per dish were observed and counted.

2.3.7 | Cell Cycle Analysis by Flow Cytometry

Six-well plates were seeded with Caco-2 cells at a density of 2×10^5 cells per well. To integrate the cells, the media was withdrawn after 24 h and they were then rinsed with PBS before being cultured for another 24 h in serum-free DMEM. After that, the cells were exposed to MPS (2 and 4 μM) in a medium that included 10% FBS. Trypsin was used to separate the cells after 24 h, followed by PBS washing and fixation in cold 70% ethanol. The transformed cells were resuspended in PBS, then treated with RNase A (100 μg/mL) for 30 min at 37°C, then stained with propidium iodide (50 μg/mL) for 15 min at 4°C. A Flow Cytometer was utilized to evaluate the location of nuclear DNA across the various cell cycle stages (BD FACS Aria Fusion, India). BD FACS Diva 9.0.1 software was used for processing and analyzing the data [39].

2.3.8 | Immunocytofluorescence Investigations on Cell Lines

Caco-2 cells (1×10^6 cells/well) were plated on glass coverslips and grown to confluency. For FisT experiments, the cells were treated with 160 μm FisT for 48 h at 37°C in the presence of 5% CO2. After incubation, these cells were fixed for 20 min with 3% paraformaldehyde and rinsed once using lukewarm PBS. then Incubated for 1 h in a blocking solution containing mouse monoclonal antibodies against Keap-1, MTOR, and DNMT-1 (1:500 dilution Abcam Pvt. Ltd.) after permeabilization with 0.2% Triton X-100 for 15 min and blocking with a solution comprising 1% bovine serum albumin and 2% normal donkey serum for 30 min. After a 12 h incubation period with a 1:100 dilution of the Alexa Fluor 488, secondary antibody from Abcam Laboratories Inc. mixed. The cells were fixed for 20 min in either 3% paraformaldehyde or methanol after being rinsed once with warm PBS for immunolabeling of Caco-2 cells cultured on cover slips. However, its interference with actin labeling, methanol fixation improved the visibility of KEAP-1, DNMT-1, and MTOR in Caco-2 cells. At the Department of Pharmacology & Toxicology, NIPER Hajipur, India, images were seen under a Zeiss microscope, taken with an Axiocam 208 color camera, and scaled for analysis using ZEN blue software version 3.4.91.0 (Zeiss Inc., Germany). Each dish included 10 randomly selected fields that were tallied and inspected. After that, Adobe Photoshop 5.0 and OpenLab2 (Improvision) were used to process the photos [40].

2.3.9 | WB Studies on Colon Cancer Cell Lines

Caco-2 cells were plated in a 75 mm^2 dish (5×10^5 cells) for 12 h, followed by treatment with FisT (160 μM and 5-Fu 20 μM) for 48 h. After treatment, cells were harvested, washed twice with PBS, and centrifuged. The membrane, cytoplasmic, and nuclear proteins were extracted from each sample in compliance with the manufacturer's guidelines. Caco-2 cells were digested by using RIPA lysis and extraction buffer (89900, Invitrogen Thermo Fisher, India) containing protease inhibitors. After that, samples were centrifuged for 10 min at 4°C at 12,000g. The BCA Protein Assay Kit (Sigma Aldrich, India) was used to measure the amount of protein in every sample. Nitrocellulose (NC) membranes (Bio-Rad Laboratories, India) were used to transfer equal quantities of protein after they had been separated using 12% SDS-PAGE. After 1 h of blocking with 5% nonfat milk, the PVDF membranes were treated with particular primary antibodies overnight at 4°C. Cellular protein samples were used to measure the expression of DNMT-1, Keap-1, & MTOR with β-actin as a loading control. Tumor tissue samples were analyzed for DNMT-1, Keap-1, & MTOR expression. After washing with Tris-buffered saline (TBS) the cell membranes were treated with an HRP-conjugated secondary antibody for 1 h after being incubated three times for 10 min. Following additional washes, an ECL WB analysis kit was used for detection in accordance with the manufacturer's instructions [37].

2.4 | In-Vivo Experimentations

2.4.1 | Animal's Experimental Design

Following global standards for animal handling & utilization, the present investigation utilized Wistar rat males weighing between 125 & 130 g. In their controlled environment, the rats were kept at 25 ± 2°C, 50% humidity, and a 12 h light/dark cycle. They were given water, a regular pellet diet, and unlimited access to food. Four groups of 10 rats each were randomly allocated to the animals. To minimize selection bias, animals were randomly assigned to treatment groups based on a computer-generated randomization schedule. This resulted in an unbiased allocation of animals between control, DMH, and treatment groups with similar body weight and baseline health status. Randomization was done before treatment initiation and conducted by a personnel investigator who was not engaged in downstream analysis. The DMH dose decided after extensive literature research and previous findings with colon cancer in same type of model. The normal control was represented by Group I. For 16 weeks, Group II had a weekly subcutaneous injection of DMH (40 mg/kg body weight). In this group, after two doses of DMH administration (Sigma-Aldrich, India), aberrant crypt foci (ACF) was induced. Group III was treated with 50 mg/kg body weight of FisT along with DMH. Group IV received 20 mg/kg 5-FU, along with DMH. All animals were fasted overnight before the final day of the study, after which they were killed, and blood and tissue samples were collected for analysis. Treatments began after the first DMH injection and continued daily until Week 16. The Institutional Animal Ethics Committee's ethical standards and NIPER-Hajipur advanced laboratory guidelines were followed when housing and caring

for the animals. The ethical approval number is NIPER-H/IAEC/41/22.

2.4.2 | Bodyweight and Growth Rate Evaluations

Body weight and growth were regularly monitored and observed during the study period. The animals were weighed starting on the first day, and then every week till they were killed. The growth rate calculated using the formula provided below [41]:

$$\text{Growth rate (\%)} = \frac{\text{Final body weight–Initial body weight}}{\text{Total number of experimental}}$$

2.4.3 | Average Tumor Volume and Number Calculation

The calculations that follow were used to get the average number of tumors, tumor volume, as well as tumor inhibition percentages [42]:

$$\text{Tumor incidence \%} = \text{No . of tumours bearing rats /number of total rats} \times 100\%$$

$$\text{The usual incidence of tumours in rats} = \text{overall tumour incidence/number of rats with tumors}$$

$$\text{Tumor volume (mm}^3\text{)} = \text{Tumour length (mm)} \times [\text{tumour width(mm)}]^2$$

$$\text{Tumors prohibition \% age} = (\text{No . of tumour in DMH group} - \text{No . of tumour in treated group /No . of tumours in DMH group}) \times 100$$

2.4.4 | Evaluation of the Disease Activity Index (DAI)

After starting DMH administration, the body weight and fecal conditions of every rat were tracked every day. Haematochezia, fecal consistency, and body weight loss were used to calculate a DAI. The sum of the three aforementioned factors was the DAI score (0–10). To analyze DAI, GraphPad Prism (version 8.0.2 GraphPad Software, San Diego, CA, USA) was used to determine the area under the curve (AUCs) for each group of experiments [43].

2.4.5 | Biochemical Assessments

The manufacturers of Rat IL-6, IL-1β, TNF-α, IL-18 ELISA kits by (Bio legend Inc. 9727 Pacific Heights Blvd. San Diego, Catalogue no. 437107, 437004, 430201) and (Elabscience United State. Catalogue no. E-EL-H0253, E-EL-H0253) followed standard technique and instructions to perform the experiments [44].

2.4.6 | Macroscopic Evaluation and Sample Collection

Colons were promptly removed, opened longitudinally, and cleaned with regular saline once the animals were fully anesthetized. The percentage of animals in each group with one or more evident of tumors was used to calculate tumor incidence. Visual macroscopic examination was used to count the number of tumors. A digital caliper was used to measure each tumor's length (l), breadth (w), and height (h). The tumor volume was then estimated ($l \times w \times h \times \pi/6$) [45]. After the inner surface of the colons had been observed macroscopically, half of the colons were flattened for polyp counting and investigation of ACF. The additional specimens were either maintained at −80°C for gene and protein expression analysis or preserved in 10% buffered formalin for histopathological and IHC investigation. People who were blind to the treatment groups conducted all laboratory measures.

2.4.7 | Histological Assessments

The whole colon was taken out, opened fully and washed with saline during sacrifices. After the cecum was removed, the remaining colon was split into three sections, each measuring 8 cm. These were called the proximal colon (next to the cecum), middle colon, and distal colon (next to the rectum). For ACF counting, each segment was flattened on filter paper in 10% buffered formalin for 24 h, followed by 20 min of 0.1% methylene blue staining in PBS. Two pathologists used a compound light microscope with a ×40 magnification to carefully examine the specimens, mucosal side up. Their distribution pattern along the colon and crypt multiplicity was scored, and the number of ACF was ascertained. For histological analysis, slices of tissue were cut perpendicular to the muscularis mucosa and stained with hematoxylin and eosin. The sample was analyzed for the presence and degree of colon cancer and dysplasia in accordance with the previously published parameters [46].

2.4.8 | WB Studies

The animals were given anesthesia at the completion of the investigation and perfused through normal saline then killed; tissue was collected, washed twice with PBS, and stored in appropriate temperature. The tissue proteins were extracted from each sample according to the previously published work. Briefly, Colon tumor tissues were homogenized using RIPA Lysis and Extraction Buffer (89900, Invitrogen Thermo Fisher, India) containing protease inhibitors. After that, the samples underwent a 10 min, 12,000g centrifugation at 4°C. The BCA Protein Assay Kit was used to measure the amount of protein in each sample (Sigma Aldrich, India). Proteins in the same quantities were separated using 12% SDS-PAGE and then transferred to membranes made of NC (Bio-Rad Laboratories, India). The membranes were blocked for an hour using 5% nonfat milk, and then they were treated with certain primary

antibodies throughout the whole night at 4°C. Cellular protein samples were used to measure the expression of DNMT-1, Keap-1, & MTOR with β-actin as a loading control. Tumor tissue samples were analyzed for DNMT-1, Keap-1, & MTOR expression. All antibodies were sourced from Abcam, India. Afterwards, three 10 min TBS washes, the membranes were incubated for an hour using a secondary antibody conjugated with HRP. After several washings, an ECL WB analysis kit was used for detection in accordance with the manufacturer's instructions [47].

2.4.9 | Immunohistofluorescence (IHF) Assessments

From the colon tissue freezing media blocks sectioned by cryostat (LEICA CM3050 S), four sections with a thickness of 5 μm were cut. The Anti-Keap1 Antibody (abcam India; Cat: A83585), MTOR (Invitrogen thermofisher India; Cat: PA5-34663), DNMT-1(Bio Genomics Asia; Cat: A19679-20μL), and Anti-Ki67 Antibody (abcam India; Cat: A104333) was used for the tests, rat monoclonal primary antibody. Before using DPX mounting solution to mount the slice, we stained the nuclei with 4,6-diamidino-2-phenylindole. Initially, 0.1% pepsin (0.01 M HCl) was used to digest the tissue for 30 min at room temperature. Following three PBS washes (pH 7.4), 10% BSA blocking media was applied for 30 min at room temperature to block it. After another PBS wash, the tissue was incubated with primary antibodies at room temperature for 12 h. Primary monoclonal antibody were incubated at ambient temperature for the whole night with 5-μm-thick sections [48, 49]. Alexa Fluor 488 is a goat anti-mouse IgG2b cross-adsorbed secondary antibody (A-21141, Invitrogen Thermofisher, India) was used for incubation the next day. Three PBS washes were used to get rid of extra antibodies. A Zeiss fluorescent microscope was used to record fluorescence pictures automatically. The tissue was then immersed in PBS (pH 11) for a whole night to eliminate the three antibodies.

2.5 | Statistical Analysis

The mean ± standard deviation was used to display the data. For multiple comparisons, both one-way and two-way analysis of variance was employed. All groups were compared using Tukey test & two-way (ANOVA) Bonferroni test. To guarantee sufficient sample size and repeatability, in vivo tumor therapy trials were conducted in triplicate in separate experiments. GraphPad Prism software 8.0 (La Jolla, CA, USA) was applied to every statistical study. The following was noted as statistically significant: $^{*}p < 0.05$, $^{**}p < 0.01$, $^{***}p < 0.001$, and $^{****}p < 0.0001$.

3 | Results

3.1 | Predicted Targets and PPT Network Evaluation

In this study, a total 1223 potential active colon cancer targets related to fisetin were obtained from GeneCards, CTD, and GediPNet as depicted in Figure 1A. As shown in Figure 1B, the venn diagram for colon cancer and FisT intersection analysis which reveals 37 shared targets between colon cancer-related genes and FisT targets which were considered as possible therapeutic targets for colon cancer. Subsequently, we constructed compound-target network and the PPI which reveals the network exposes the relationships between major FisT-targeted proteins (Figure 1C,D). Further, we performed biological process enrichment analysis, depicted in Figure 1E, the biological processes which is considerably enriched among FisT targets, including apoptosis, cellular stress responses, and RNA-mediated gene silencing. Figure 1F shows molecular function enrichment analysis which depicts enhanced molecular activities, including cytokine binding, DNA binding, and xenobiotic transport, with targets organized by fold enrichment. Figure 1G depicts cellular component enrichment analysis, which includes extracellular vesicles, plasma membrane regions, and nuclear structures. At last, we performed KEGG pathway enrichment analysis which shows pathways that are enriched among FisT targets, such as cancer signaling pathways, AGE-RAGE signaling in diabetic complications, and p53 signaling pathways (Figure 1H). Ultimately, KEAP-1, DNMT-1, and mTOR regarded as the critical effector targets of FisT against colon cancer.

3.2 | FisT Shows Highest Docking Score With KEAP-1, DNMT-1, & mTOR Proteins

Figure 2A–C and Table 1 representing that FisT has significant interactions with the target proteins in the docking investigation, with variable binding affinities as indicated by binding energies. The molecule had a binding energy of −7.92 kcal/mol with mTOR that was stabilized by hydrogen bonding and other stabilizing factors, especially engaging residues CYR2243 and SER2355 inside the active site. FisT demonstrated a somewhat higher affinity for DNMT1, with a binding energy of −8.16 kcal/mol, which was predominantly maintained by crucial hydrogen bonds and hydrophobic interactions involving the PRO1223 and GLN1226 residues. Notably, FisT has the most affinity for KEAP1, with a binding energy of −9.26 kcal/mol. The interaction was characterized by strong hydrogen bonding and π−π stacking with key residues ASN382 and VAL512 at the active site. Collectively, these data highlight FisT potential as a modulator of these protein targets, with Keap1 showing the highest affinity.

3.3 | Molecular Dynamics Simulation (DNMT1−FisT Complex)

A 100 ns molecular dynamics simulation was performed to study the structural and dynamical behavior of the DNMT1 protein in a complex with FisT. To assess the stability and interactions within the protein−ligand complex, the most important parameters to measure are root mean square deviation (RMSD), radius of gyration (Rg), root mean square fluctuation (RMSF), solvent-accessible surface area (SASA), and hydrogen bonding patterns. The results are described in detail below in (Figure 3A–F).

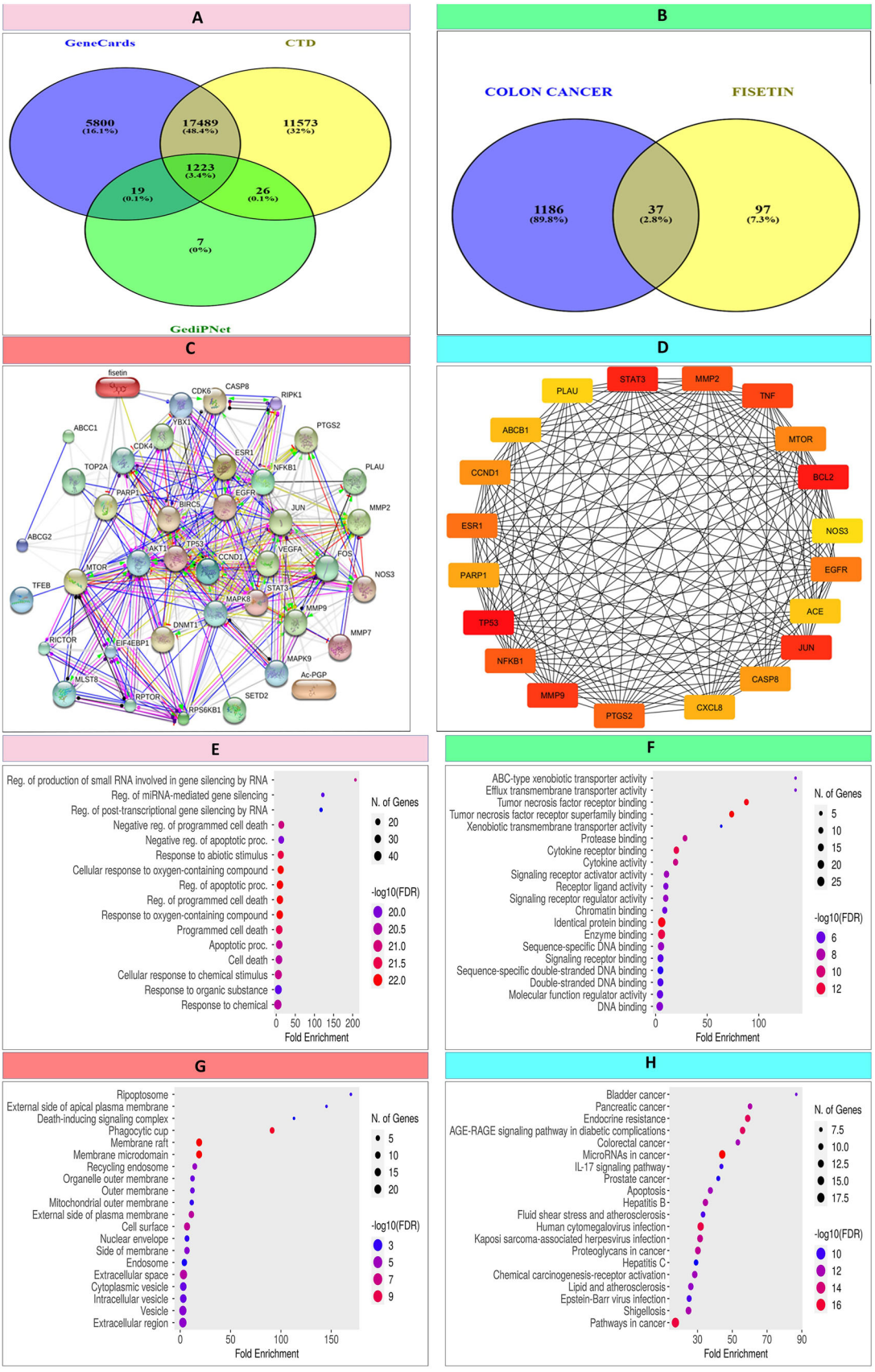

FIGURE 1 | Legend on next page.

3.3.1 | RMSD

Figure 3A representing the MD simulation exhibits a stable protein−ligand interaction. The RMSD plot reveals that the protein backbone (black line) is constant (0.3−0.4 nm) for 100 ns with no considerable conformational change. The ligand (red line) possesses higher RMSD (1.0−2.2 nm), showing flexibility or minor repositioning within the binding pocket, which is satisfactory for dynamic interaction. The RMSD plot indicates the structural stability of the protein and that of the ligand during the time course of the simulation. In the provided plot, the protein backbone RMSD (black line) is always low, between 0.3 and 0.4 nm, for the course of the 100 ns simulation. This means that the protein structure is conformationally stable with minimal deviations or unfolding throughout the process of ligand binding. A stable RMSD less than 0.5 nm is usually taken to reflect a well-structured and stiff protein structure at physiological conditions. The fact that there are no big fluctuations or steep peaks indicates that the protein has equilibrated and that binding of the ligand does not create any destabilizing conformational changes. This stability enhances the credibility of the binding interaction seen in the molecular docking and support for the suitability of the complex for potential biological assessment.

3.3.2 | RMSF

Figure 3B,C shows the RMSF plot which highlights the flexibility of individual residues in the protein and ligand during the simulation. Specific regions of the protein, such as loops or terminal ends, exhibited higher RMSF values (up to 1.5 nm) are indicative of intrinsic flexibility. These regions are likely located away from the ligand-binding site. In contrast, the residues within and around the binding pocket showed lower RMSF values, indicating restricted movement due to direct interactions with FisT. The ligand itself displayed moderate RMSF values, reflecting its ability to adapt to the binding pocket while maintaining stable interactions with the protein.

3.3.3 | Rg

Figure 3D is representing the Rg provides the numerical estimation of the compactness and general folding state of the protein structure during the course of the molecular dynamics' simulation. It represents the spread of the atomic mass from the center of mass of the protein. In the reported plot, the overall Rg (black line) remains fairly constant during the 100 ns simulation, oscillating narrowly between 3.75 nm, which implies that the protein is in a compact and stable conformation throughout time. Biologically, stability of Rg implies that the protein does not experience significant conformational unfolding or dilation, even when in the presence of the ligand. The Rg along the x, y, and z axes (red, green, and blue lines, respectively) also exhibit controlled variations, showing small local rearrangements but no large-scale structural collapse or instability. In general, an Rg of < 0.2−0.3 nm variation with respect to time is acceptable for a stable globular protein. The lack of a consistent upward or downward trend further confirms the structural integrity of the protein−ligand complex throughout the simulation. In addition to RMSD, the Rg analysis assures that ligand binding does not interfere with the native fold of the protein, reinforcing the compound's appropriateness for biological purposes.

3.3.4 | SASA

Figure 3E is showing that the SASA analysis measures the solvent exposure of the protein−ligand complex. Throughout the simulation, the sum of SASA decreased slightly from approximately 590−570 nm^2. This decline implies that the protein-probe complex is significantly more compact on binding than in its isolated state; this may be a result of conformational changes that more profoundly hide hydrophobic regions from solvent access. These changes further support the stability of the protein−ligand complex, and the ligand may influence the surface dynamics of the protein.

3.3.5 | Hydrogen Bonding Analysis

Hydrogen bonding proves to be very important for stabilization of protein−ligand complexes. The analysis represented that the DNMT1-FisT complex held 2−8 hydrogen bonds in all the simulations. In fact, this was an indication of dynamic interactions wherein, constantly, formation and breaking within time were observed. These hydrogen bonds are significant for fixing FisT in the binding pocket and hence significantly contribute to the affinity and stability of the complex. Distributions of hydrogen bond donor−acceptor distances mainly lay in the vicinity of 0.25−0.35 nm. This range falls in the range of the typical distance of strong hydrogen bonds and, therefore, confirms strong interactions between the protein and the ligand. The narrow distribution implies these interactions are stable and specific. The MD simulation outcome indicates that FisT firmly binds to the DNMT1 protein and gives stable complexation. Stability in the protein structure is indicated by slight changes in the conformation of the protein upon ligand binding. High Rg and SASA values along with stabilized hydrogen bonding patterns suggest the strong affinity of FisT in the binding pocket. In conclusion, these findings render FisT a candidate molecule for further biochemical and functional studies concerning DNMT1 (Figure 3F).

FIGURE 1 | Network pharmacology: Elucidating complex fisetin−target interaction of colon cancer. The illustration above depicts a network pharmacology approach investigation and evaluating Fisetin therapeutic potential in colon cancer. (A) Combines data sets to identify common targets, whereas (B) focuses on the junction of colon cancer genes with fisetin targets. (C) Exhibits fisetin target network, whereas (D) shows protein−protein interactions within these targets. (E, F, G, and H) Provide enrichment studies that reveal key biological processes, molecular activities, cellular components, and signaling pathways. This comprehensive review emphasizes the probable methods via which fisetin may exert therapeutic effects on colon cancer.

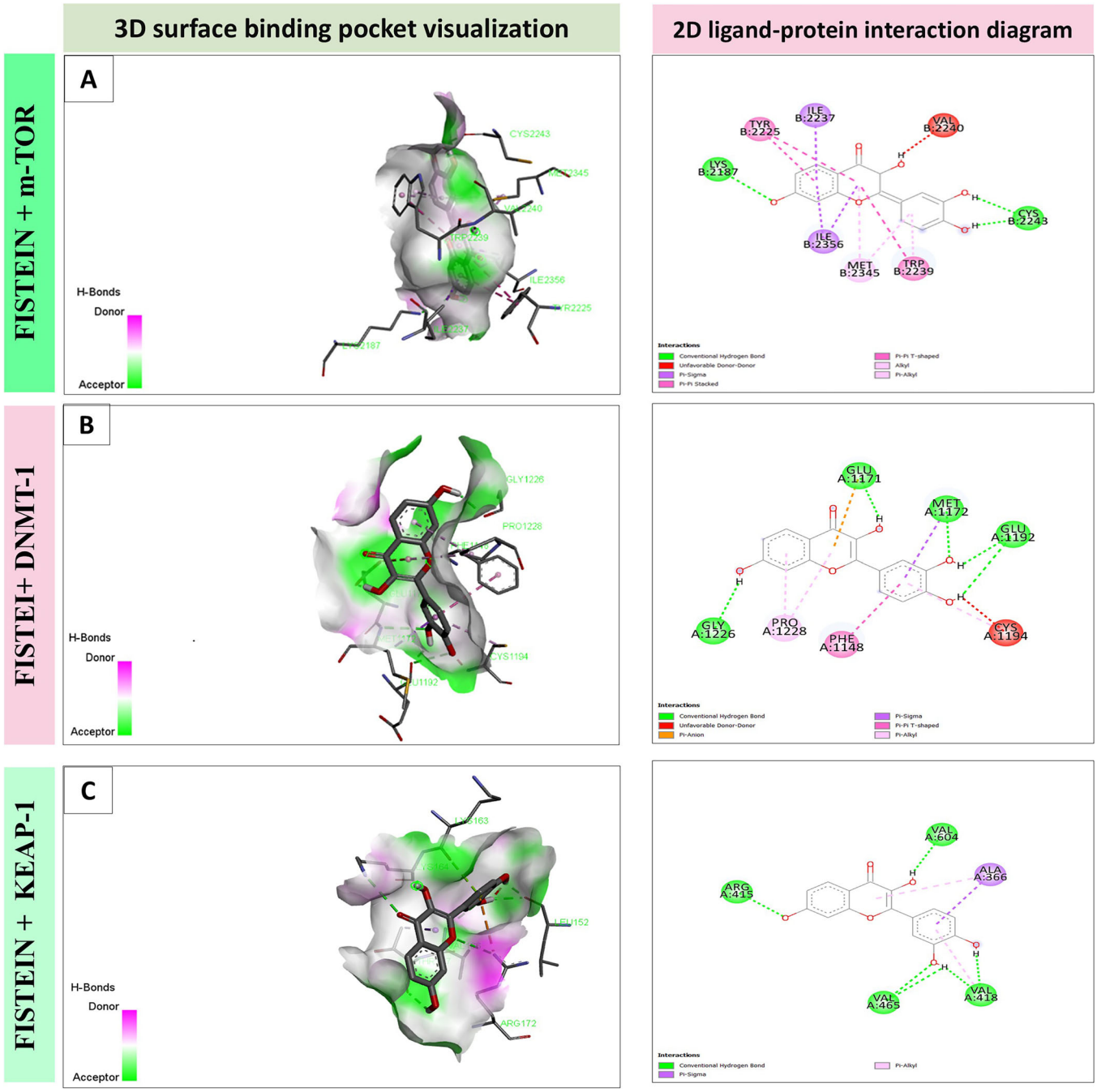

FIGURE 2 | In silico prediction of ligand–protein interaction of fisetin. (A) Fisetin interacts with mTOR. Due to hydrogen bonding and other stabilizing interactions within the active site, the residues CYR2243 and SER2355 add a significant contribution. (B) Fisetin-DNMT 1: Important hydrogen bonding and hydrophobic interactions occur, involving in particular PRO1223 and GLN1226. (C) The complex of Fisetin bound to Keap-1 shows crucial hydrogen bonds and π–π stacking with key residues at the active site, including ASN382 and VAL512. The 3D (left) and 2D (right) visualizations depict binding pocket characteristics and residue-level interactions, supporting the potential of fisetin as a modulator of these protein targets.

3.4 | Effect of FisT Against Cell Viability Assay and 2D Cellular Morphology

(Figure 4A–F) shows the cell viability of HCT16, Caco-2, & CT26 cells treated with different concentrations of FisT and 5-FU for 48 h. Both FisT and 5-FU decreased the viability and cellular growth ($p < 0.001$) (Figure 5C,I) of the cell lines ($p < 0.001$) depending on the dosage when used alone. FIST and 5-FU showed IC50 = 160 μm and 20 μm, respectively, on Caco-2, HCT116, and CT-26 cell lines.

3.5 | FisT Showing ROS Production & DNA Fragmentation

ROS production is directly associated with DNA fragmentation and apoptosis. Figure 5A,J,E,H showing the ROS production is higher DCF fluorescent intensity after treated with FisT and 5-fu up to 60%, 55%, and 26%, respectively in different treatment groups. The significant different were observed ($p < 0.001$) when compared with the control group.

FisT-induced apoptosis was investigated using an apoptosis assay as the pharmacodynamics endpoint of cancer therapy (Figure 5B,D) illustrates the % age of DNA fragmentation after FisT intervention. DNA fragmentations on Hoechst staining on cell after treated with FisT group were seen higher when compare to the cancerous control group, FisT significantly ($p < 0.001$) increased apoptosis. 5%, 51.12%, and 42.26% when compared to the control group, FisT significantly ($p < 0.001$) increased apoptosis.

Our research proves that FisT substantially increases ROS levels, resulting in DNA fragmentation and apoptosis in colon cancer cells. In particular, DCF fluorescence intensity was up approximately 50%−60% in FisT-treated groups, reflecting increased ROS production (***$p < 0.001$). This is corroborated by Russo et al. [50], who established that fisetin causes apoptosis in colon cancer cells via ROS-mediated mechanisms. In addition, Hoechst staining showed enhanced DNA fragmentation, where apoptosis levels were 51.12% in FisT-treated cells versus 5% in controls (**$p < 0.001$). These findings are in agreement with the findings of Pandey et al. [51], who reported that fisetin-induced ROS generation triggers mitochondrial dysfunction and apoptosis in CRC cells. Your research builds on this knowledge by presenting quantitative evidence of ROS levels and rates of apoptosis, adding support for FisT as a multi-targeted anticancer drug in the treatment of CRC.

TABLE 1 | Fisetin docking score with selected protein targets against colon cancer.

Serial no	Protein target	Docking score
1.	m-TOR	−7.92
2.	DNMT-1	−8.16
3.	KEAP-1	−9.26

3.6 | FisT Exhibited Antiangiogenic Effect Against 2D Colon Cancer Cell Lines

(Figure 5G,K) shows the Caco-2 developed colonies after 10 days of treatment. The percentage of colony formation for Control, FisT, & 5fu was 97%, 45%, and 50%, respectively. Colony formation significantly decreased (***$p < 0.001$) in FisT-treated and 5-FU-treated group when compared to the control group.

3.7 | Antimetastatic Activity of FisT on 2D Cell Lines

The migration assay of Caco-2 CRC cells was investigated by cell migration assay. In the Caco-2 cells treated with 160 μm (***$p < 0.001$) of FisT were found to prohibit the migration of aggressive cells up to 45%−50% when compared with the control group (Figure 6E,F).

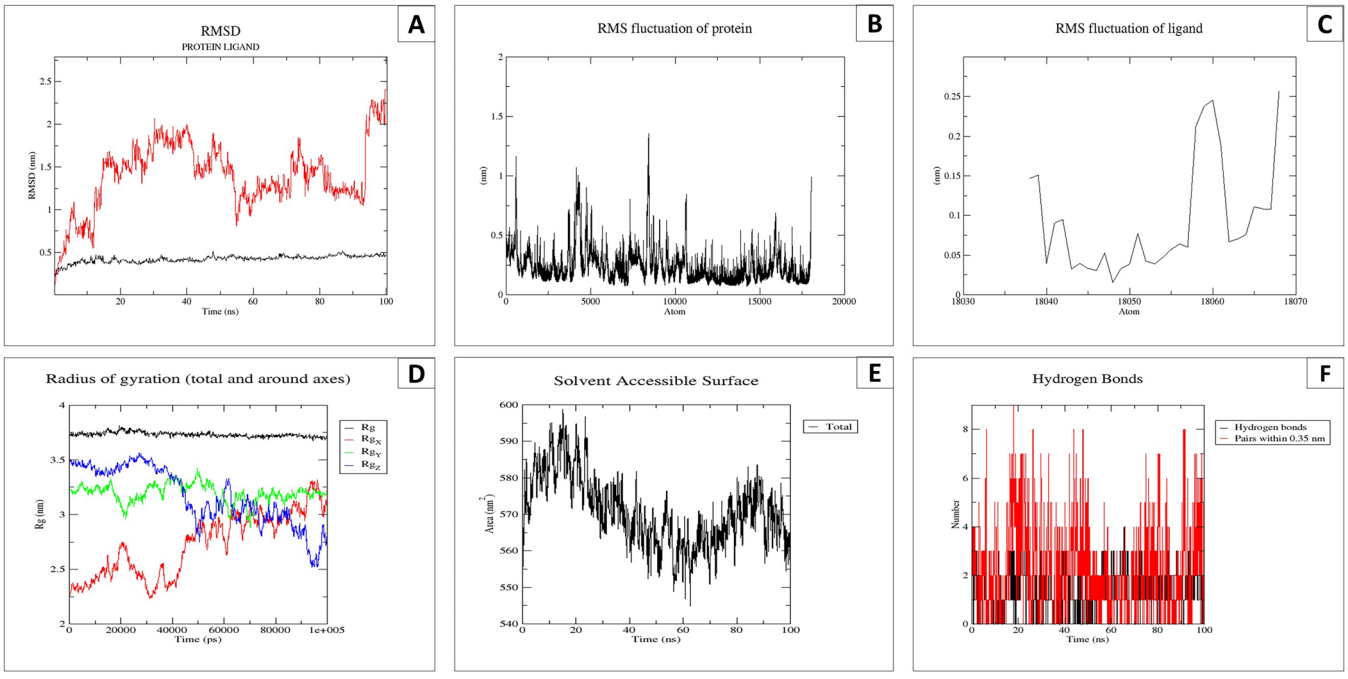

FIGURE 3 | Unveiling dynamic protein−ligand interaction and conformational landscape of fisetin. (A) RMSD of the protein−ligand complex shows that the binding interaction is stable, and the ligand RMSD is minimal. (B) RMSF of the protein residues indicates regions of structural flexibility, which show stable binding pockets. (C) RMSF of the ligand is minimal, suggesting a consistent positioning within the binding site. (D) The radius of gyration (Rg) analysis reveals the compaction and stability of the protein throughout the simulation. (E) Solvent accessible surface area (SASA) measurement of the exposure of the protein changes within the simulation. (F) Hydrogen bond analysis frequency and stability between fisetin and DNMT1, indicating the latter's strong binding affinity (Table 1), Fisetin docking score with colon cancer specific targets.

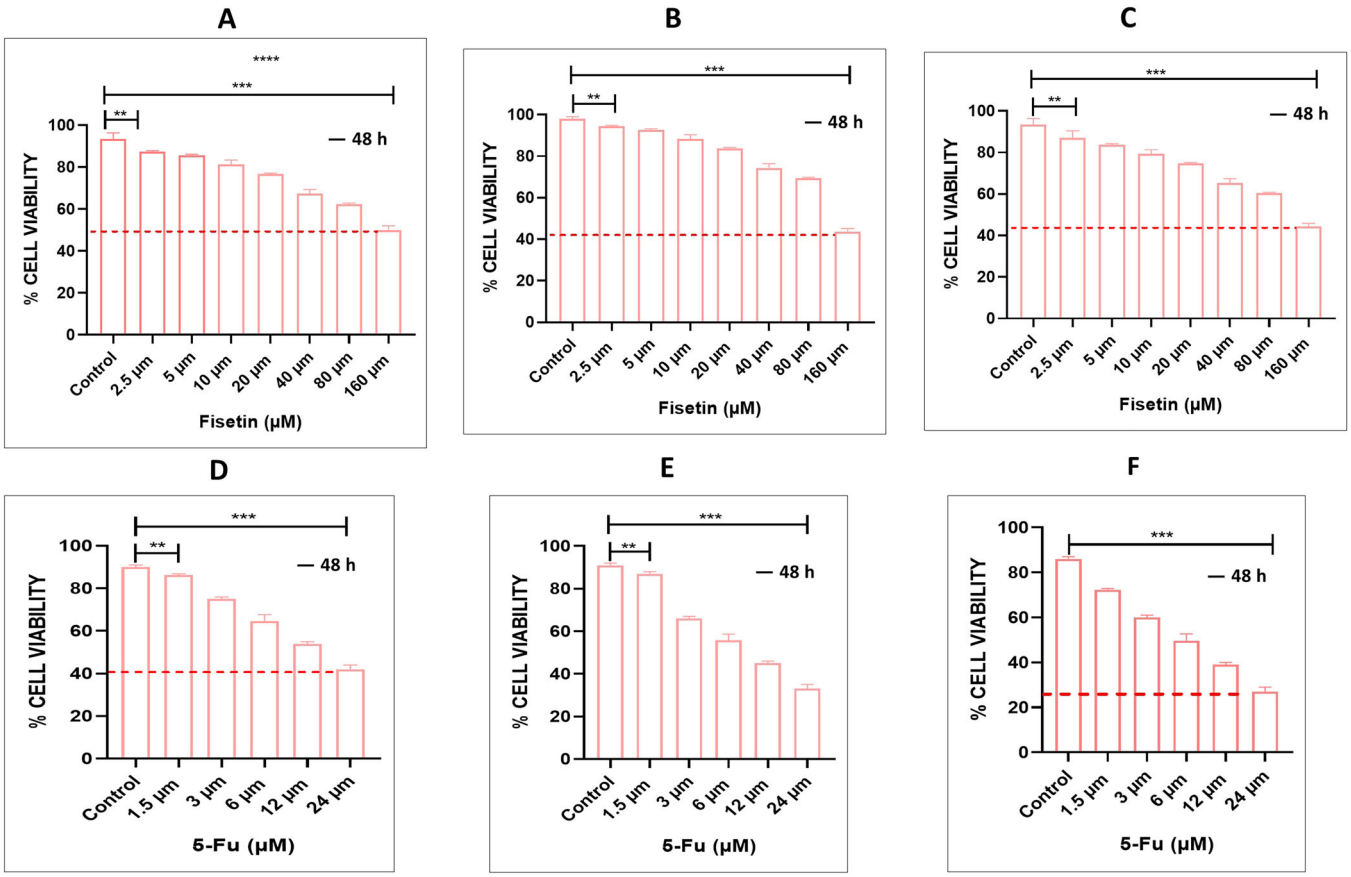

FIGURE 4 | IC50 concentration of selected compounds. (A–C) Fisetin IC50 against CACO-2, HCT116, & CT26 cell lines. (D–F) 5-FU IC50 against CACO-2, HCT116, & CT26 cell lines. Error bars represent mean ± SD ($n = 3$). *$p < 0.05$, **$p < 0.01$, ***$p < 0.001$, and ****$p < 0.0001$ versus control. Each performed in triplicate by one-way analysis of variance (ANOVA) Turkey's posttest. ns; not significant.

3.8 | FisT Inhibited KEAP-1, DNMT-1, and mTOR Expression in Human Cell Lines

The network pharmacology study revealed considerable enrichment of the KEAP-1, DNMT-1, and mTOR pathways. It is well recognized that the KEAP-1, DNMT-1, and mTOR pathways play an important role in tumor growth. We anticipated that fisetin might have therapeutic benefits by enhancing the expression levels of KEAP-1 and down-regulated DNMT-1, and mTOR in colon cancer cell lines, which we tested using immunocytofluorescence and WB analysis. As described in Figure 6A–D. Figure 7A,B,E,F, Control group shows higher expression when compared with the FisT group. FisT significantly enhanced the expression levels of KEAP-1 and downregulated the DNMT-1 and mTOR expression levels. These findings suggested that FisT might lower the protein expression levels of DNMT-1, mTOR, and overexpress the KEAP-1 level, resulting in a therapeutic impact on colon cancer cell lines.

Our results concur with research like Zamanian et al. [7]. and Fialková et al. [8]., which showed the effect of polyphenolic compounds on single oncogenic pathways. Wherein our research works supersedes this information by demonstrating concerted downregulation of KEAP-1, DNMT-1, and m-TOR in both in vitro (HCT-116 cells) and in vivo (DMH-induced colon cancer rat model) using immunocytofluorescence and WB analysis. Such two-model support fortifies the argument for FisT as a highly effective multi-targeted therapy for CRC.

3.9 | FisT Arrested Cell Cycle on G1/G0, S, & G2/M Stages

Proliferation is associated with the cell cycle. The G1/G0, S, and G2/M phases of the cell cycle can be distinguished based on the DNA content measured by PI staining on flow cytometry facilities instrument at central instrumentation facilities NIPER-Hajipur. As shown in (Figure 7C,D), in the PBS control group, some cells arrested in the G0/G1 phase. However, the percentage of cells arrest was 55% in G0/G1 phase, 37% in S phase, and 32% in G2/M phase was observed after treatment with FisT treated group drug concentrations (160 μM) after 48 h of treatment. Moreover, FisT were shown to enhanced the cell cycle arrest in different treatment group ($p < 0.001$) when compared with control group. The induction of cell cycle arrest by FisT was consistent with their antiproliferative effect, the prohibition of cell cycle stages could have induced inhibition of colon cancer cell proliferation.

Our results are consistent with research such as that conducted by Barra et al. [52] and Zamanian et al. [12] which

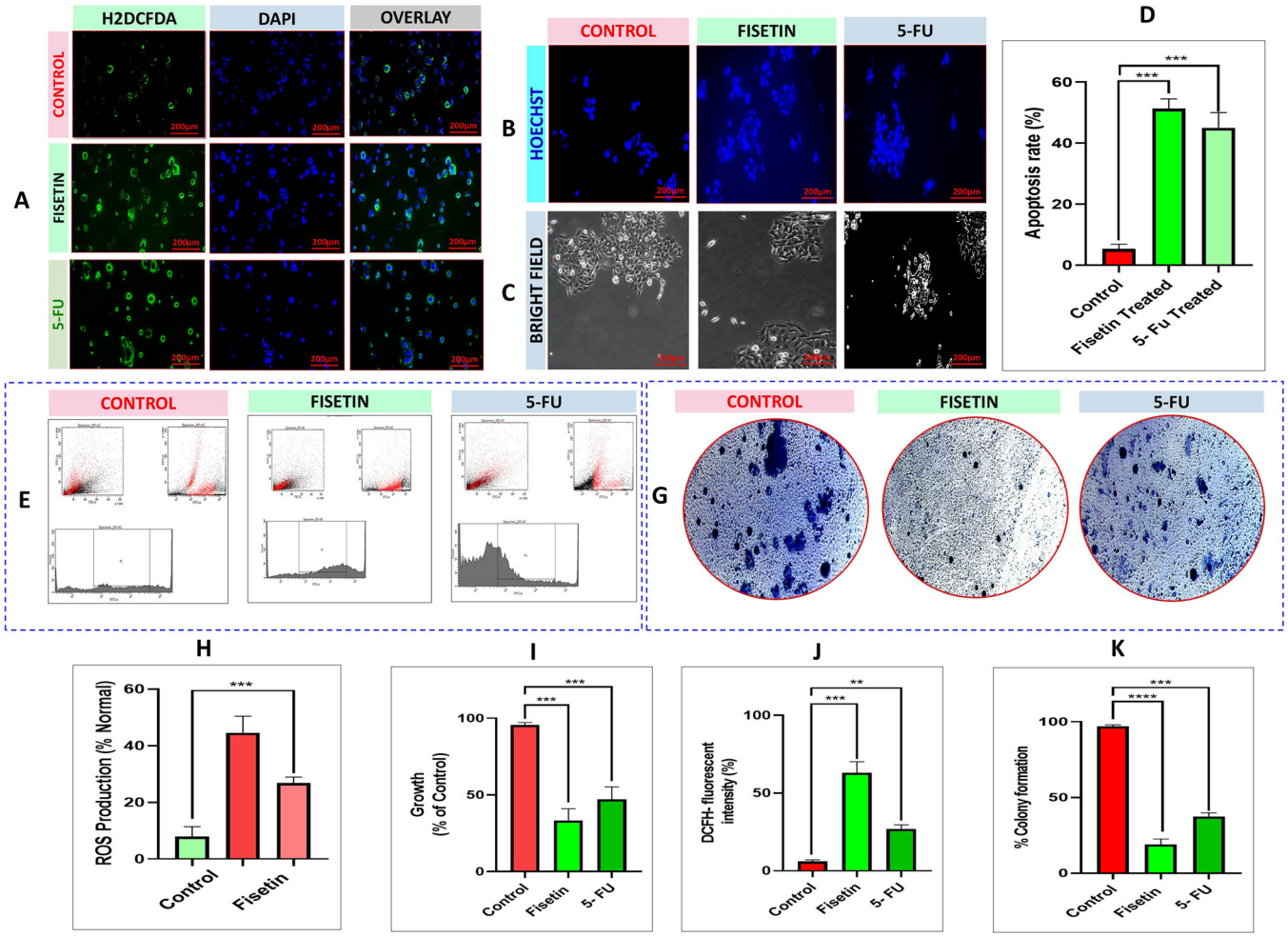

FIGURE 5 | Fisetin prohibited cancer cell growth via ROS production, colony formation, and apoptosis in cell lines. (A, J) Representing ROS production fluorescent images and % of ROS production. (B, D) Condensed DNA and apoptosis rate during treatment. (C, I) Showing the reduction in cellular growth. (F) Mechanistic insight of Hoechst staining. (E, H) Indicating the higher ROS production in fisetin-treated group. (G, K) Indicating the reduction in the number of colonies in fisetin group. Error bars represent mean ± SD ($n = 3$). *$p < 0.05$, **$p < 0.01$, ***$p < 0.001$, and ****$p < 0.0001$ versus control. Each performed in triplicate by one-way analysis of variance (ANOVA) Turkey's posttest. ns; not significant.

indicated the Fisetin-induced only G2/M arrest in colon cancer cells. but our research builds upon this understanding by showing accurate phase distribution (G0/G1: 55%, S: 37%, G2/M: 32%) against 160 μM FisT following 48 h, confirmed by flow cytometry, and correlating this with antiproliferative effects such as colony formation assay and cell migration assays. This rigorous, phase-by-phase profiling within a set concentration-time paradigm confers greater translational significance to the mechanism of action of FisT.

3.10 | FisT Improved Body Weight in DMH Treated Colon Cancer Rats

The significant effect of FisT on the experimental animal's body weight fluctuations is shown in Table 2. Notably, as compared to the control group, the DMH-treated rats showed a statistically significant and noticeable decrease in their ultimate body weight, weight gain, and growth rate ($p < 0.001$; ***$p < 0.001$). On the other hand, the body weight dynamics of DMH-activated rats were significantly improved by the administration of FisT. Interestingly, the FisT dosage of 50 mg/kg/BW was observed to significantly increase the ultimate body weight and growth rate of DMH-triggered mice and dramatically ameliorate weight loss compared to the DMH-treated group (Figure 8).

3.11 | Antitumour Response of FisT on Tumor Characteristics on Macroscopic and Microscopic Analysis (Goblet Cells, ACF, & Adenoma)

Figure 9A–E depicts the emergence of cancers of the colon, histological alterations, ACF, mast cell alterations, and reduced number of goblet cells triggered by DMH. Group II rats received DMH alone showed 100% colon tumor growth. Number of polyps seen higher (***$p < 0.001$) when compared to normal control rats, whereas FisT treatment in Group III and 5fu treatment in Group IV resulted in the reduction in number of tumor polyp and ACF incidence and seen improvement in number of goblet formation, tumor

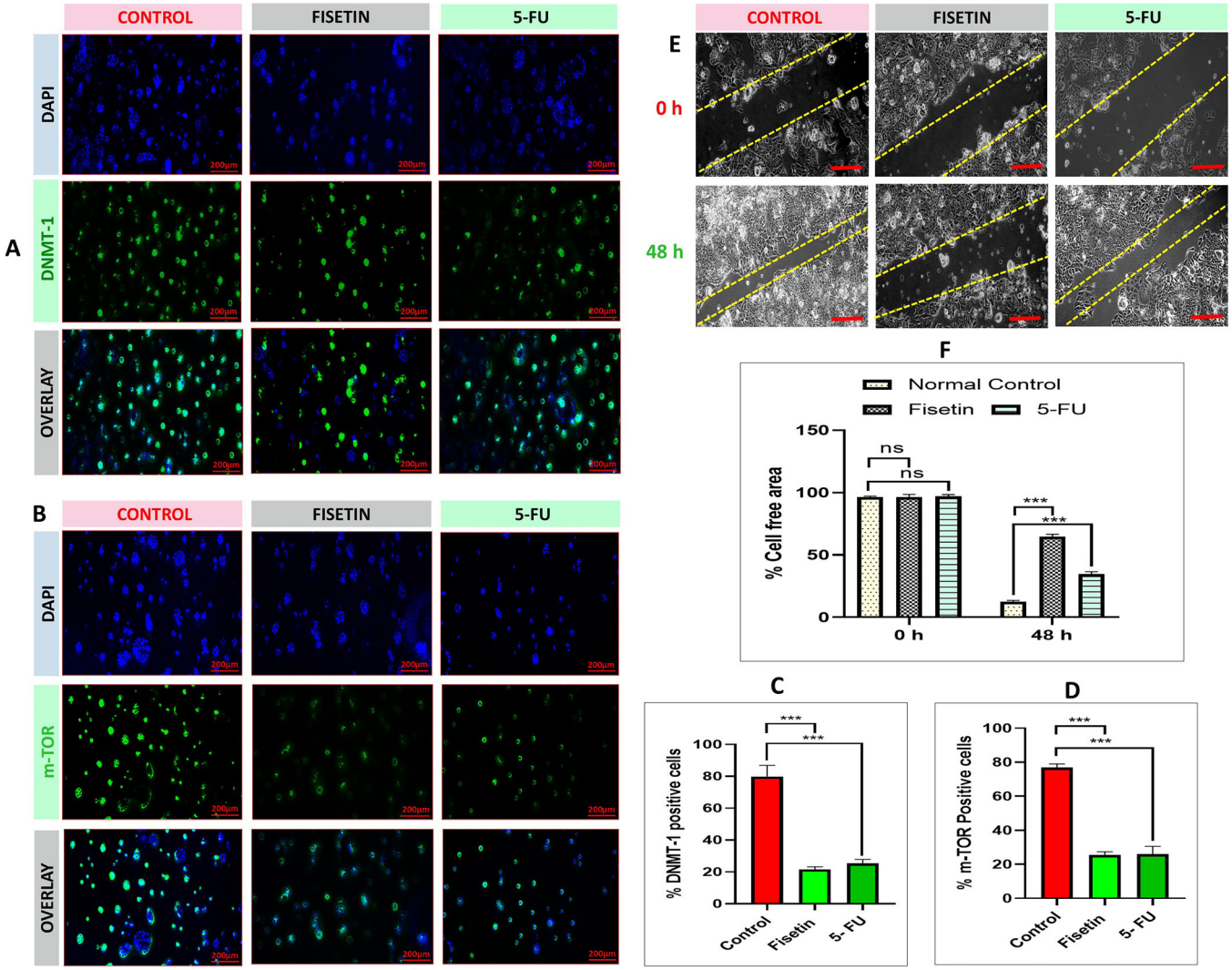

FIGURE 6 | Fisetin suppresses DNMT-1 activity and reduces mTOR expression in human colon cancer cell lines. (A, C) Representative photographs of the immunofluorescence staining for DNMT-1 by Alexa Flour 488 secondary antibody (green) and the DAPI staining (blue; for nucleus) in fisetin (200 μM), 5-fu (20 μM) compared with cancer control cell lines. (B, D) Immunocytofluorescence analysis of mTOR activity in control, fisetin-treated, & 5-fu-treated Caco-2 cell lines. (E, F) Representing the % cell free area on fisetin-treated & 5-fu-treated compared with untreated control cells. Error bar represents means ± SD of three separate experiments; *$p < 0.05$, **$p < 0.01$, ***$p < 0.001$, and ****$p < 0.0001$ versus control. Each performed in triplicate by one-way analysis of variance (ANOVA) Turkey's posttest and two way (ANOVA) Bonferroni test. ns; not significant.

volume and size also tumor incidence, no of tumors and percentage of tumor inhibition has been improved in treatment group (Tables 3 and 4), and so forth (***$p < 0.001$; Figure 9A–E). When compared to rats treated with DMH alone, the number of polyps was limited and found to be lower in rats treated with FisT.

This is in alignment with other research, such as do Nascimento et al. who saw a decrease in ACF, mitotic index, and histopathological abnormalities [53] and Xiao et al. [54] and Xiao et al. who saw inhibition of ACF and inflammation. But our research progresses this by not just limiting ACF and tumor burden but also restoring goblet cells, inhibiting mast cell infiltration, lowering tumor volume, and linking histological restoration to molecular markers (Ki67, mTOR, DNMT1, KEAP1), thereby demonstrating a more general, multi-targeted chemo preventive effect of FisT within a single in vivo model of colon cancer.

3.12 | FisT Potentially Modulated the Inflammatory Pathways in Colon Cancer Model (IL-6, IL-1β, TNF-α, IL-18)

IL-6 rises throughout colon cancer growth and development, encouraging tumor formation and persistent inflammation. Then, TNF-α and IL-18 increases, causing tissue damage and inflammation exacerbated. Tissue damage is indicated by a spike in the level of CPK along with a reduction in SOD and GPx antioxidant enzymes when oxidative stress increases up. Colon cancer develops as a result of a microenvironment that fosters tumor development and progression due to ongoing inflammation, oxidative stress, and tissue damage. Level of IL-6 were higher in DMH-treated group when compared to normal control and FisT has shown to decreased the level of IL-6 (***$p < 0.001$; Figure 10E) when compared to the DMH-treated group. TNF-α were seen higher (***$p < 0.001$; Figure 10F) when compared to DMH-treated group then FisT intervention

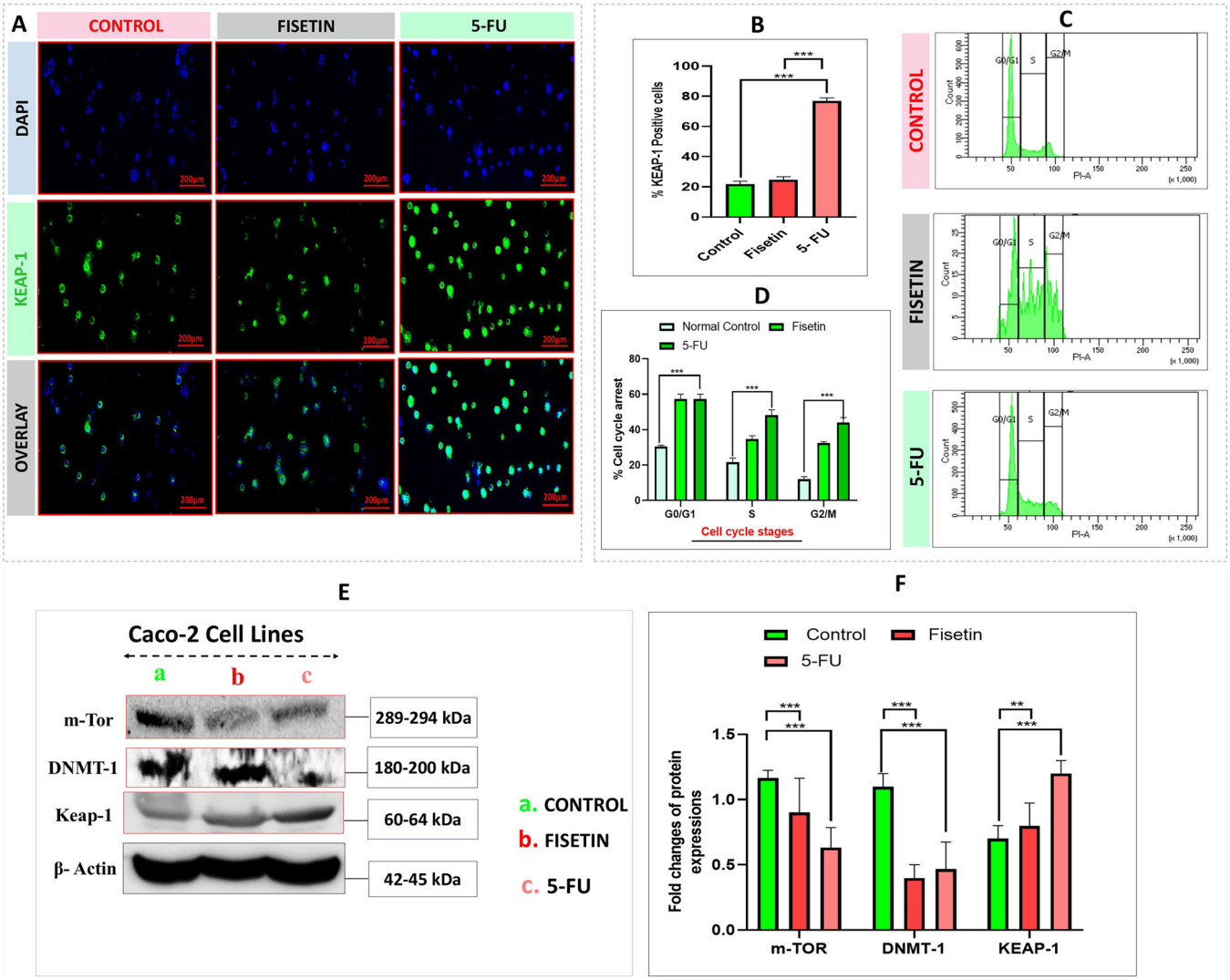

FIGURE 7 | Fisetin modulated MTOR, DNMT-1, & Keap-1 in colon cancer cell lines (A, B). Representative photographs of the immunofluorescence staining of Keap-1 (green) and the DAPI staining (blue; for nucleus) in fisetin (200 μM), 5-fu (20 μM) compared with cancer control cell lines. (C, D) The percentage of cell arrest in G1, S, and G2/M of cell cycle when treated with fisetin (E, F). Western blot analysis for differential protein levels of markers MTOR, DNMT-1, and Keap-1 in fisetin and 5-fu-treated in vitro. Error bar is means ± SD of three separate experiments. $^{*}p < 0.05$, $^{**}p < 0.01$, $^{***}p < 0.001$, and $^{****}p < 0.0001$ versus control. Each performed in triplicate by one-way analysis of variance (ANOVA), Tukey test, and two-way (ANOVA) Bonferroni test.

TABLE 2 | Fisetin effect on body weight changes and growth rate in colon cancer model.

Groups	Initial body weight (g)	Final body weight (g)	Weight gain (g)	Growth rate (%)
Control	125.74 ± 6.59	257.19 ± 11.42*	131.45 ± 7.62	104.54 ± 0.06*
DMH	123.45 ± 5.61	189.65 ± 8.26*	66.2 ± 7.26	53.63 ± 0.09*
Fisetin + DMH	129.59 ± 4.81	227.69 ± 10.91*	98.1 ± 6.91	75.69 ± 0.03*
5-FU + DMH	125.77 ± 5.15	248.87 ± 8.15*	123.1 ± 8.15	97.87 ± 0.05*

downregulated the TNF-α level ($^{***}p < 0.001$; Figure 10F) when compared with DMH group. IL-1β were seen higher ($^{***}p < 0.001$; Figure 10G) when compared to DMH-treated group then FisT intervention downregulated the IL-1β level ($^{***}p < 0.001$; Figure 10G) when compared with DMH group. IL-18 were seen higher ($^{***}p < 0.001$; Figure 10H) when compared to DMH-treated group then FisT intervention downregulated the IL-18 level ($^{***}p < 0.001$; Figure 10H) when compared with DMH group. FisT supplementation significantly reduced the elevated levels of IL-6, TNF-α, IL-1β, and IL-18; from the above outcomes, we can say that FisT has potential to overcome the progression of tumors in DMH-treated rats.

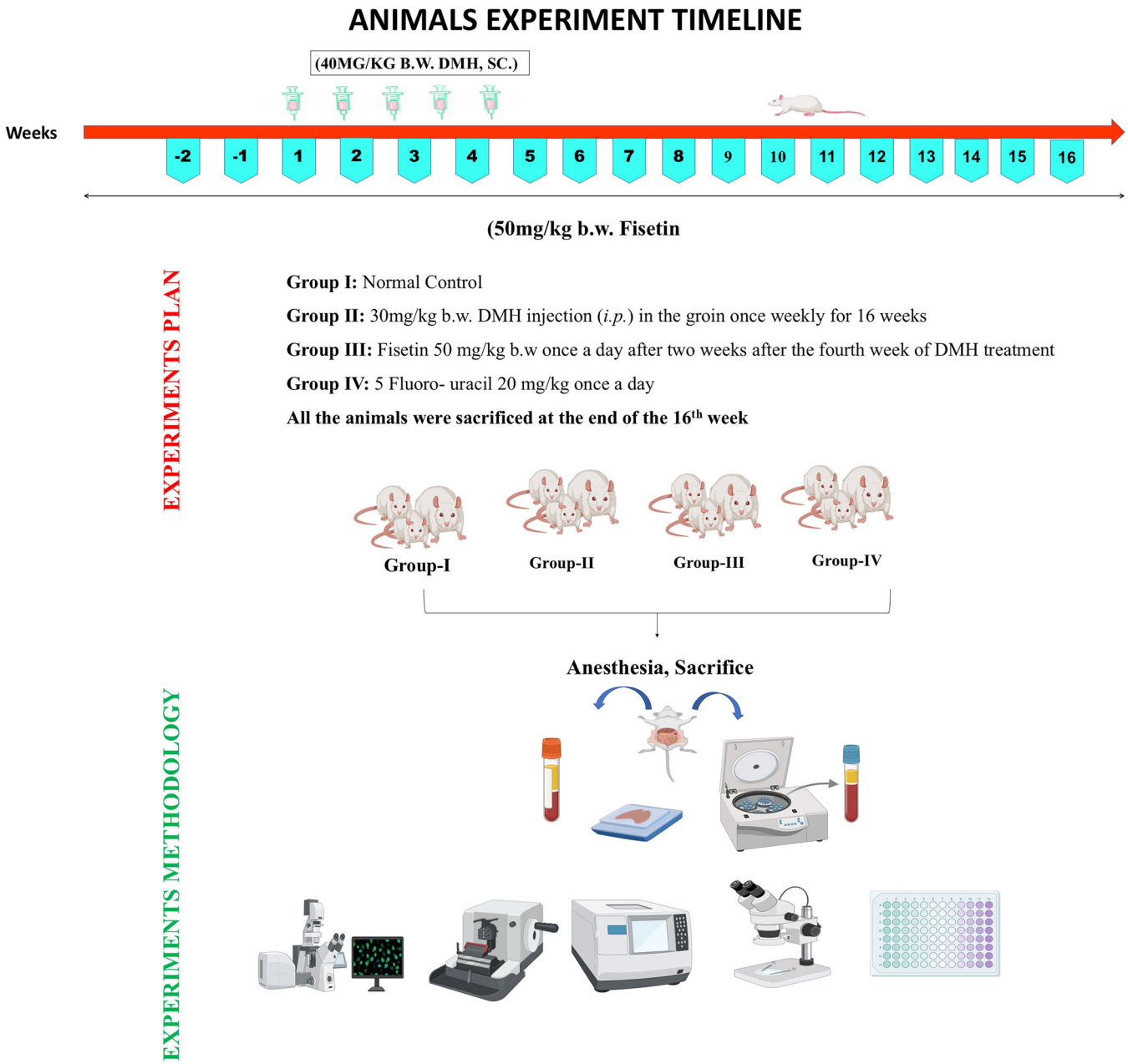

FIGURE 8 | Experimental design and group classification.

This is consistent with the work of Sahu et al. [55] and Farsad-Naeimi et al. [56], which documented fisetin's anti-inflammatory activities through NF-κB inhibition. Our work, however, improves on the existing findings by showing concomitant modulation of multiple pro-inflammatory cytokines in a chemically induced colon cancer model and cancer cell lines, demonstrating FisT's greater efficacy as a multi-targeted anti-inflammatory and anticancer drug in the treatment of CRC.

3.13 | FisT Upregulated KEAP-1 and Downregulated DNMT-1, mTOR, and ki67 Expression in DMH Treated Rats

The network pharmacology study revealed considerable enrichment of the KEAP-1, DNMT-1, and mTOR pathways. It is well recognized that the KEAP-1, DNMT-1, and mTOR pathways play an important role in tumor growth. We anticipated that fisetin might have therapeutic benefits by modulating the expression levels of ki67, KEAP-1, DNMT-1, and mTOR in colon cancer animal model, which we tested using IHF and WB analysis. As described in Figure 10C,D, overexpression assessed by IHF and WB, ki67, KEAP-1, DNMT-1, and mTOR, Figures 11A–D and 12A–D, in DMH groups when compared with the normal control group. FisT significantly reduced the expression levels of mTOR, ki67, DNMT-1, and upregulated KEAP-1 level in DMH induced preclinical colon cancer model. These findings suggested that FisT may have potential to lower the protein expression levels of ki67, DNMT-1, mTOR, and overexpression of KEAP-1 (Figure 10C,D) resulting in a positive therapeutic potential on colon cancer animal model. Our results are consistent with

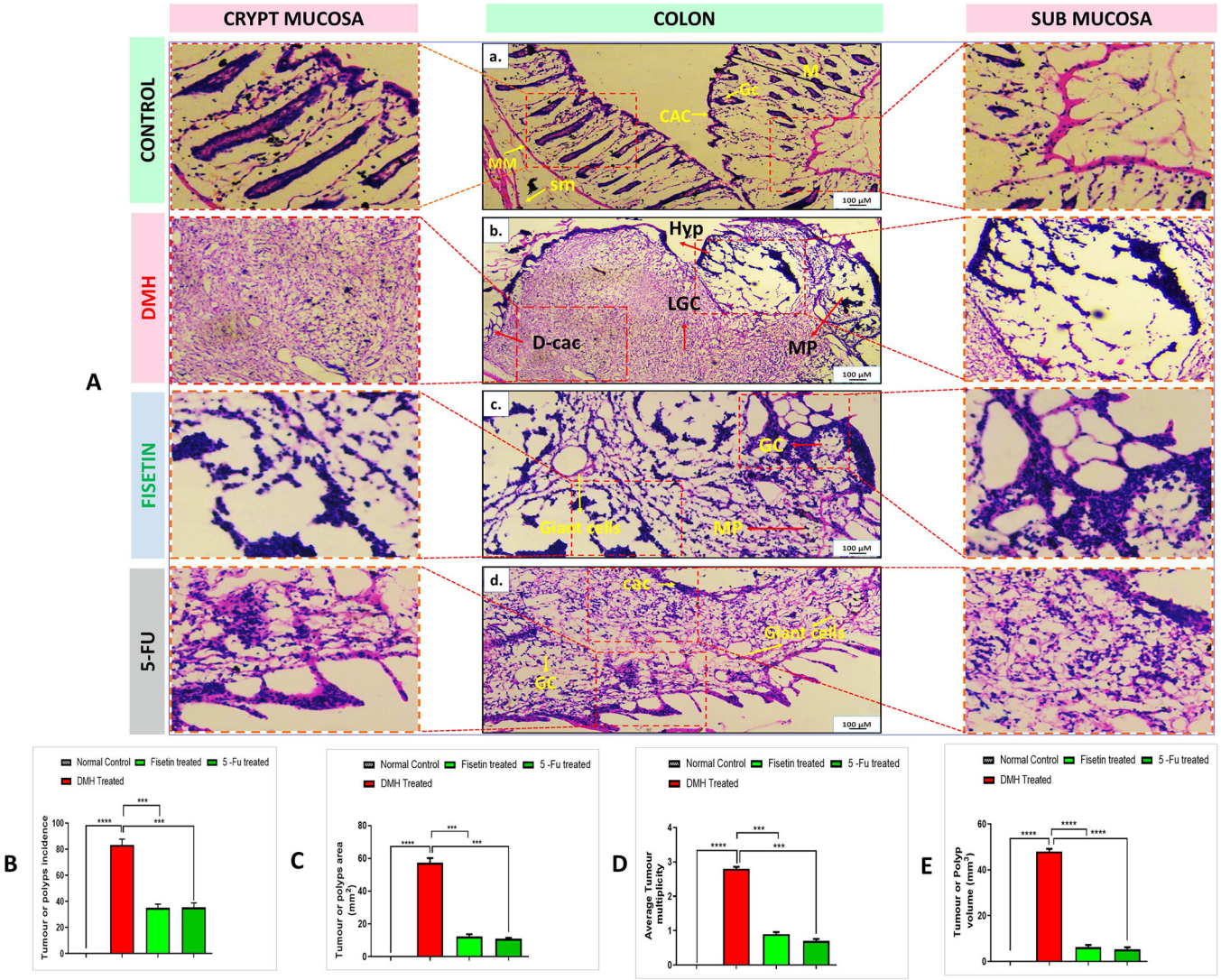

FIGURE 9 | Fisetin improved colonic tissue on DMH induced colon cancer model. (A) (a) The mucosa of normal control group denoting mucosa (M), submucosa (Sm), muscularis mucosa (MM), columnar absorptive cells (CAC), goblet cells. (b), Hyp (hyperplasia), metaplasia (MP) Distortion of CAC, hyperplasia (Hyp) and loss goblet cells (LGC). (c) Seen improved goblet cells, less metaplasia, reduction of giant cells numbers denoted by red arrow of colon mucosa treated with 50 mg/kg Fisetin DMH treated groups. (d) The colon mucosa of animals treated with 20 mg/kg of 5-FU shows normal goblet cells, proper columnar absorptive cells and less number of giant cells and less metaplasia seen, (B) Tumour or polyps incidence, (C) Tumour or polyps area, (D) Average Tumour multiplicity, and (E) Tumour or Polyp volume; Error Bar is means ± SD of three separate experiments. *$p < 0.05$, **$p < 0.01$, *$p < 0.001$, and ***$p < 0.0001$ vs. control.

TABLE 3 | The effect of fisetin against polyp's formation in colon cancer model.

Groups	Total no of rats	Number of polyps bearing rats	Total number of polyps	Percentage of polyp inhibition (%)
Control	10	0.00	0.00	Nil
DMH	10	10.00	20.00	0.00
Fisetin + DMH	10	6.00	7.00	65.00
5-FU + DMH	10	7.00	8.00	60.00

Cai et al. and other researchers [57]. wherein they have employed DMH-induced models of colon cancer specifically targeting either proliferation markers such as Ki-67 or single-pathway targets such as mTOR or DNMT1, with little known regarding modulation of KEAP1. Our work extending to the above result and shows co-suppression of mTOR, DNMT1, Ki-67, and induction of KEAP1, depicting a holistic multi-targeted modulation by fisetin (FisT), with better therapeutic

TABLE 4 | Tumor incidence (%), average number of tumors, tumor volume, and tumor inhibition percentage in DMH-induced CRC in rats.

Group (mg/kg)	No of rats	Number of tumor bearing rats	Total number of tumors	Tumor incidence (%)	Average number of tumors/tumor bearing rats	Volume of tumors (mm^3)	% of tumor inhibition
Control	10	0	0	0	0	0	0
DMH	10	10	27	100	2.7 ± 0.95	140.55 ± 0.65	0
Fisetin + DMH	10	4	12	40.0	1.2 ± 0.65	104.34 ± 0.75	55.00 ± 0.45
5-FU + DMH	10	3	10	30.04	1.0 ± 0.55	102.43 ± 0.65	62.96 ± 0.35

significance by targeting the oxidative-epigenetic-oncogenic pathway.

3.14 | Estimation of DAI

The mean number of rectal bleedings, feces uniformity, with weight loss is known as the DAI. The following were the precise scoring criteria: Body weight loss scores were 0−4, with 0 denoting no weight loss, 1 1%−5% weight loss, 2 5% −10% weight loss, 3 10%−15% weight loss, and 4 greater than 15% loss of weight. Similarly, stool consistency scores ranged from 0 to 4, where 0 represented normal stool, 1 represented moist or sticky stool, 2 represented soft stool, 3 represented soft stool with mild diarrhea, and 4 represented diarrhea only; The bleeding from the rectal score was calculated on a scale of 0 to 4, where 0 represented no blood in the stool, 1 represented Hemoccult positive, 2 represented Hemoccult positive with visual pellet, 3 represented moderate blood, and 4 represented excessive bleeding (***$p < 0.001$; Table 5).

4 | Discussion

According to a thorough analysis of the molecular processes by which Keap-1, DNMT-1, and mTOR affect CRC in both in vitro and in vivo models, FisT, a naturally occurring flavonoid that is abundant in strawberries and bok choy, may have therapeutic potential to treat colon cancer Notably, the parent molecule has been thoroughly investigated in several clinical studies up to this point, indicating its potential as a cutting-edge therapeutic moiety for the management of CRC. Such as: (https://www.cancer.gov/clinicaltrials/NCI-2022-08061, https://www.cancer.gov/clinicaltrials/NCI-2023-06774, and https://www.cancer.gov/clinicaltrials/NCI-2021-13203, proved to be significantly effective against the colon cancer, orally seen available at colonic site and enhanced colonic tissue binding (in vivo). Inhibition tests in three colon cancer cell lines and a wide panel of NCI-60 cancer cell lines demonstrated the molecule's unique therapeutic potential as a single therapeutic agent against cell lines such as HCT116, CACO-2, & CT26 and also evaluated in vivo DMH induced colon cancer model. In parallel, in recent years, FisT and its other flavonoids compounds have been extensively studied as anticancer compound [58]. However, the specific effects and mechanistic insights of FisT against colon cancer via KEAP-1, DNMT-1, & mTOR axis are still rarely explored in colon cancer. However, these evidence suggested us to implement the network pharmacology to search for the networking association between FisT with colon cancer target proteins such as KEAP1, MTOR, & DNMT1. Further, we performed molecular docking, MDA with DNMT-1, followed by in vitro and in vivo anticancer assessments. The downregulation of KEAP-1 and upregulation of DNMT-1, and mTOR a key player in the colon tumorigenesis, and in previous findings only individual or some of its associated targets were assessed for the elucidation of the potential molecular basis related to the chemo preventive property of FisT. Figure 13 shows the mechanistic flow of KEAP1, m-TOR, & DNMT1 axis plays a

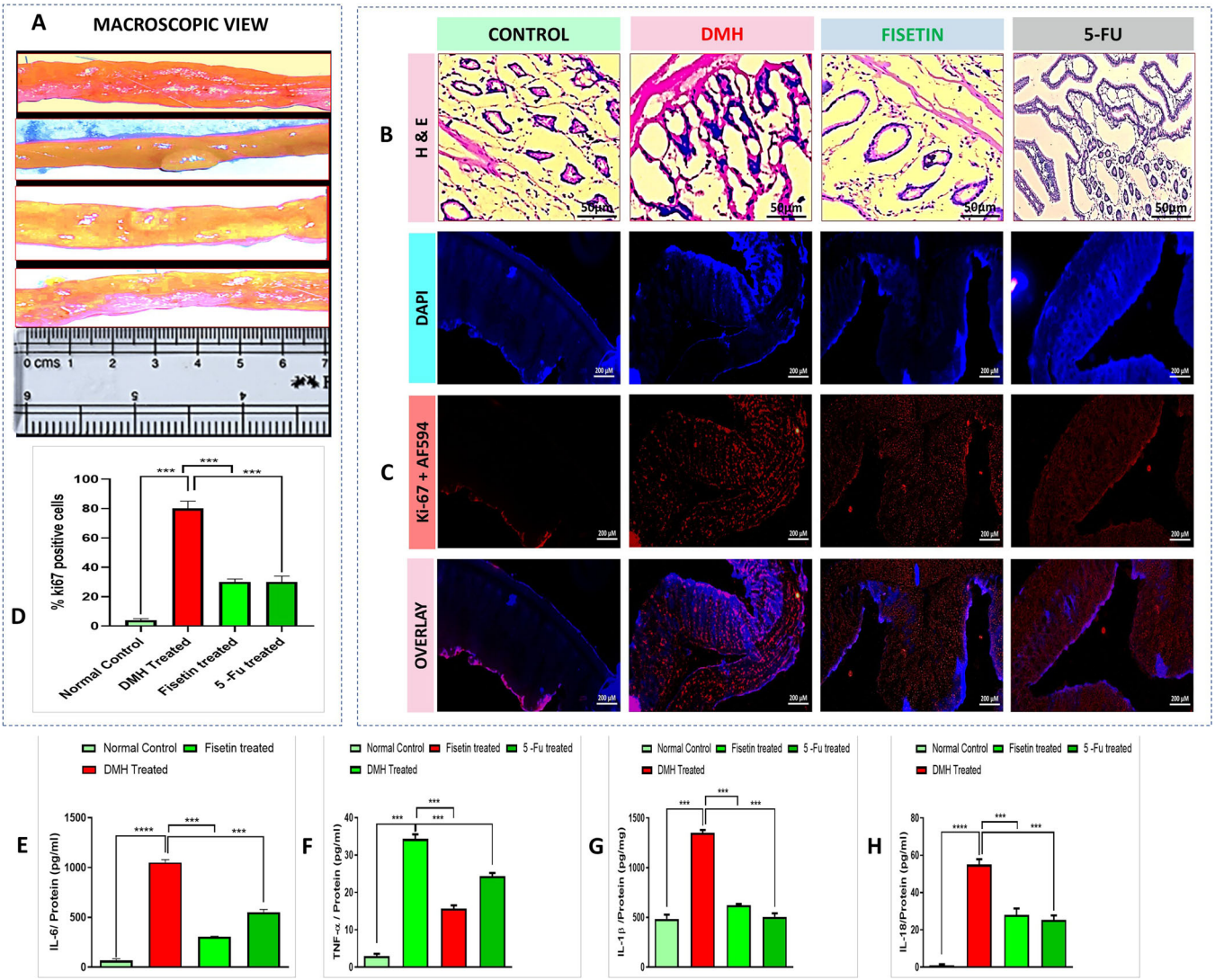

FIGURE 10 | Macroscopic, histological, and immunoassays of fisetin-treated rats. (A, B) Indicating the presence of tumor in DMH treated group. (C, D) Fluorescence imaging confirmed positive staining with a red tint. DMH group showed elevated Ki-67 immunopositive staining compared to the normal control group. Fisetin treatment lowered Ki-67 immunopositive staining. (E–H) Representing the level of pleiotropic cytokine interleukin-6, pro-inflammatory cytokines such as interleukin-18, TNF-α, and IL-1β expression in all groups. Error bar is means ± SD of three separate experiments. $*p < 0.05$, $**p < 0.01$, $***p < 0.001$, and $****p < 0.0001$ versus control.

crucial role in colon cancer development and progression. Downregulation in KEAP1, a tumor suppressor protein, lead to the binding with NRF2 and prohibiting it's translocation into the nucleus and cause ubiquitination of NRF2 leading to the degradation by proteasome also enhanced the phosphorylation of NRF2, which is necessary for translocating into the nucleus, this leads to the hypermethylation of DNMT1 [59]. Activated DNMT1, in turn, upregulates mTOR expression through HSPB8 and BAG3, which leads to colon cancer development and progression. Studies shown that KEAP1 mutations are frequent in colon cancer and are associated with poor prognosis [60]. Furthermore, activation of KEAP1 and inhibition of m-TOR & DNMT1 has been shown to suppress colon cancer cell growth and induce apoptosis in previous findings but cross talk between these pathways was not explored [61]. Therefore, targeting and exploring the KEAP1, MTOR, & DNMT1 axis together may provide a novel therapeutic strategy for colon cancer treatment to overcome the pathways' redundancy and therapy resistance in colon cancer. DMH altered the expression of KEAP1, mTOR, and DNMT1 in the colonic tissue. However, FisT, especially at the therapeutic dose, enhanced the KEAP1 and downregulated the m-TOR & DNMT1 protein expression levels. To get strong evidence, we have proved against in vitro and in vivo preclinical colon cancer model. Besides, FisT also inhibited the major pro-inflammatory cytokines such as IL1-β, IL-6, TNF-α, and IL-18. FisT, particularly at 50 mg/kg, decreased the number of tumor incidence, reduces ACF in the current investigation when compared to the control group and DMH group [62]. Weight loss brought on by colon cancer comprises several causes. Such as pro-inflammatory cytokines produced by the tumor promote cachectic factors and muscular atrophy. Nutrient absorption and metabolism are disrupted by hormonal changes, changes in the gut microbiota, and increased energy expenditure. Weight loss is caused by inflammation-

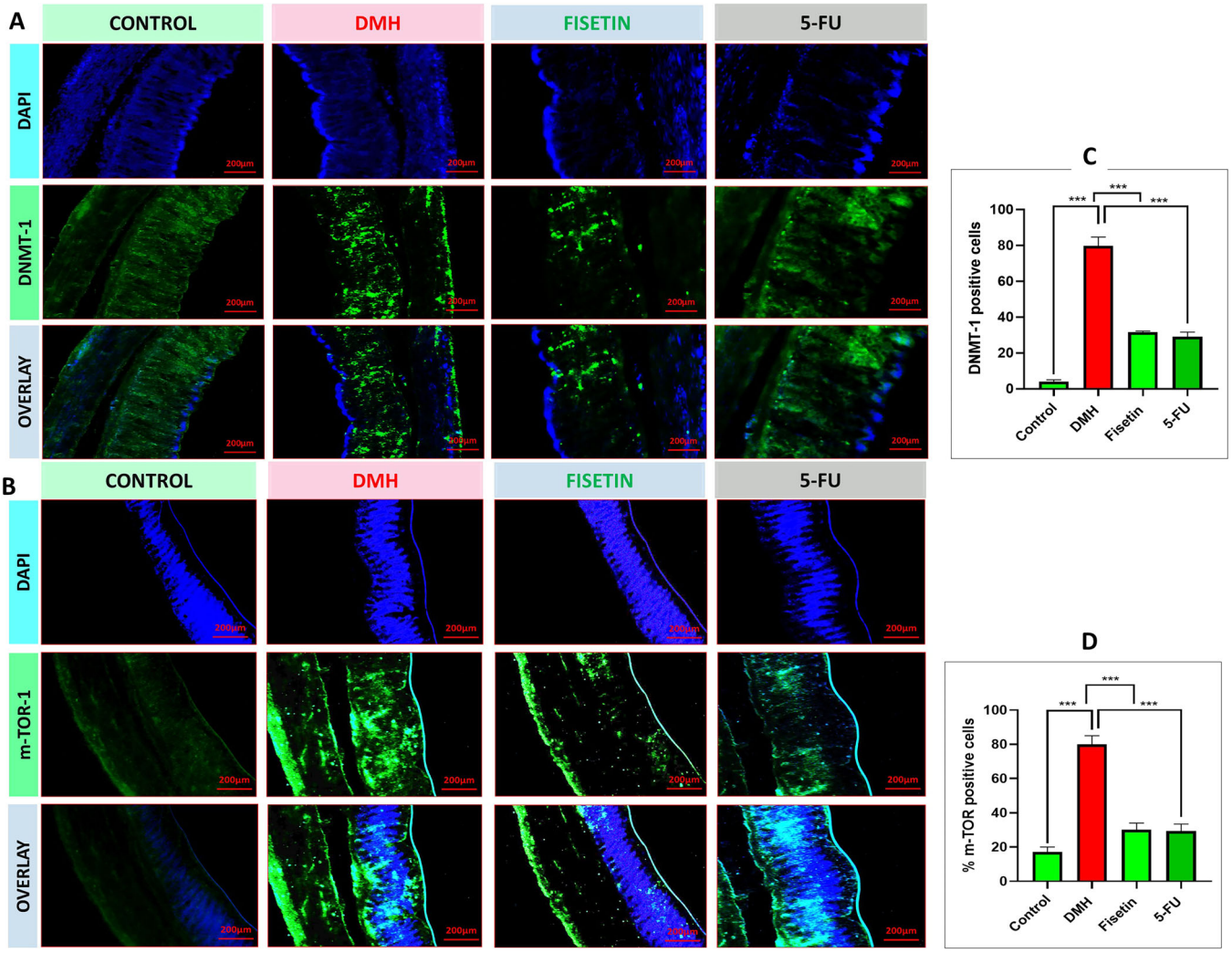

FIGURE 11 | The immunohistofluorescence analysis of MTOR & DNMT-1 expression. (A–D) Positive staining is shown by green color under fluorescence microscopy. The colonic portion of the DMH-treated control group exhibited elevated DNMT-1 and MTOR expression immunopositive staining compared to the Normal control. Fisetin-treated reduced DNMT-1 and MTOR immunostaining. The error bar represents the average ± SD of three consecutive studies. $^{*}p < 0.05$, $^{**}p < 0.01$, $^{***}p < 0.001$, and $^{****}p < 0.0001$ compared to control. Each was conducted in triplicate using a one-way analysis of variance (ANOVA) Tukey test. ns indicates not significant.

induced insulin resistance and epigenetic changes that alter gene expression [63]. Weight loss is a crucial symptom to address in cancer care because of these intricate relationships, which also contribute to the notable weight loss seen in colon cancer patients [64]. In this study, we also evaluated FisT contributing weight gain in colon cancer model. Through transforming & stimulating subsequent targets, mTOR pathway hyperactivity which enhances the progression of the cell cycle and prevents apoptosis, whereas KEAP-1 upregulation results in the loss of mTOR pathway negative regulation. DNMT-1 overexpression silences tumor suppressor genes, such as p21 and p27, through DNA hypermethylation, promoting cell cycle progression and inhibiting apoptosis [65, 66]. We have explored cell cycle analysis and apoptosis with FisT molecules the result was significant when compared with disease control group. Despite altering several kinds of histological characteristics, the KEAP1, m-TOR, & DNMT1 work together to encourage the beginnings and progression of colon cancer [67]. Activation of the mTOR pathway, specifically through the PI3K/AKT/mTOR axis, leads to the recruitment and activation of mast cells through the release of stem cell factor (SCF) and vascular endothelial growth factor (VEGF) [68]. Additionally, DNMT-1-mediated DNA hypermethylation silences the MUC2 gene, leading to depletion of goblet cells and impaired mucin production [69]. The formation of ACF is also promoted through the activation of the wnt/β-catenin pathway, which is improved by the mTOR/KEAP-1 pathway [70]. Furthermore, the interplay between the KEAP1, m-TOR & DNMT1 contributes to tumor growth and progression by regulating cell proliferation, survival, and angiogenesis through the activation of downstream targets, such as S6K1, 4E-BP1, and HIF-1α, leading to increased tumor size and volume, and promoting the development and progression of colon cancer [71]. Our in vitro results revealed that FisT inhibited the proliferation of colon cancer cells, including HCT116, CT26, and Caco-2 cells, in a dose- and time-dependent manner. FisT treatment at 160 μM induced

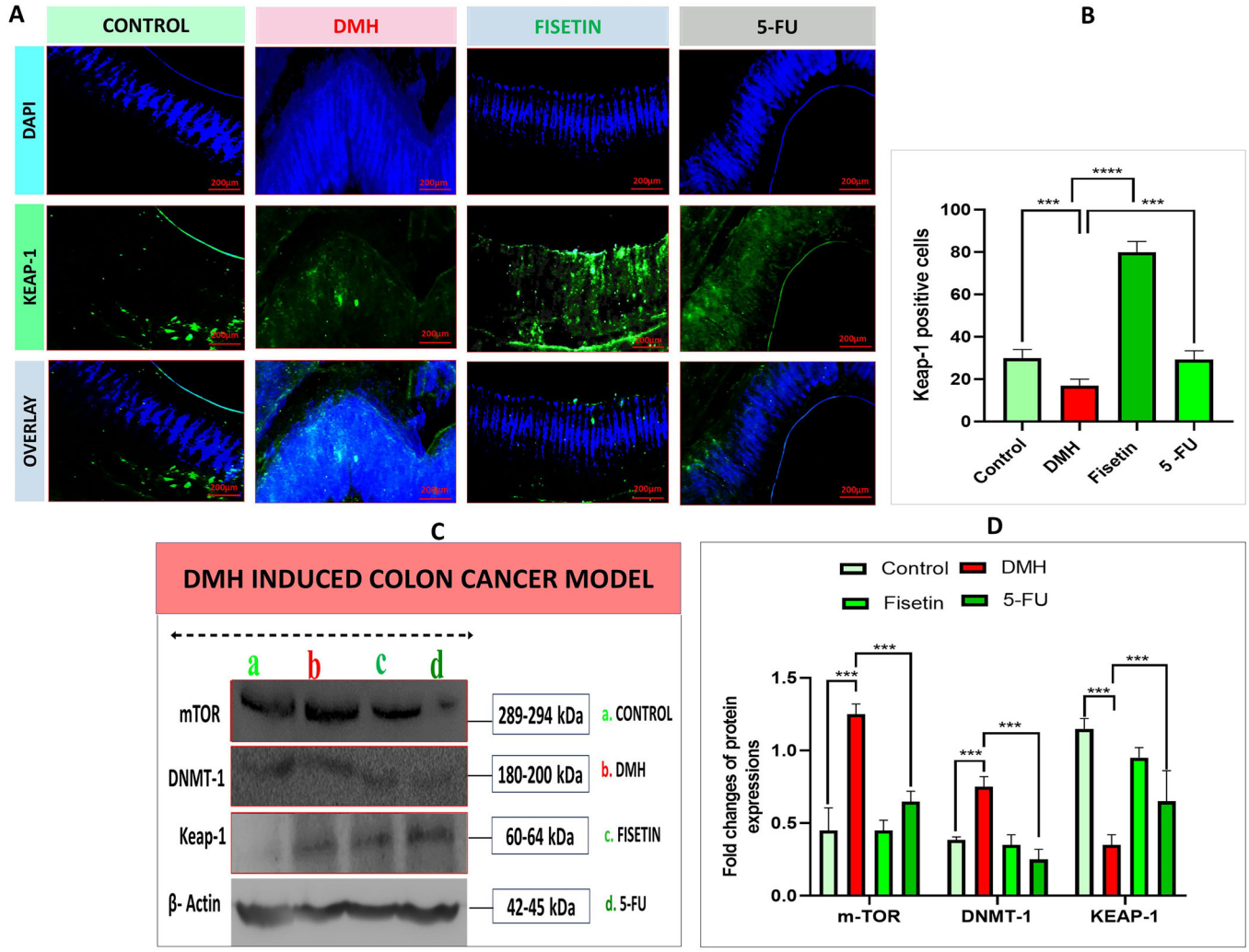

FIGURE 12 | Fisetin modulated the expression of epigenetics, signaling, and oxidative stress markers in colon cancer cell lines. (A, B) Representative photographs of the immunohistofluorescence staining for Keap-1 (green) and the DAPI staining (blue; for nucleus) in fisetin (50 mg/kg), 5-fu (20 mg/kg) compared with normal control group. (C, D) Western blot analysis for differential protein levels of markers MTOR, DNMT-1, and Keap-1 in fisetin and 5-fu-treated in vivo DMH-treated colon cancer model. Error bar is means ± SD of three separate experiments. $^{*}p < 0.05$, $^{**}p < 0.01$, $^{***}p < 0.001$, and $^{****}p < 0.0001$ versus control. Each performed in triplicate by one-way analysis of variance (ANOVA) Tukey test and two way (ANOVA) Bonferroni test. ns; not significant.

TABLE 5 | Disease activity index scoring system based on body weight loss, fecal consistency, and haematochezia.

Weight loss		Stool consistency		Blood in stools	
Observation	**Score**	**Observation**	**Score**	**Observation**	**Score**
≤ 2%	0	Normal	0	No blood	0
3%–6%	1	Semi-solid	1	Rarely seen	1
7%–12%	2	Pasty stool	2	Not seen	0
> 12%	3	Blackish and hard stool	3	Not seen	0

Caco-2 cell apoptosis. We also discovered that FisT could increase intracellular ROS levels in Caco-2 colon cancer cells. The expression of MTOR and DNMT-1 were down-regulated and Keap-1 expression was found upregulated in Caco-2 cells. These results were further confirmed in in vivo study, as FisT treatment suppressed DMH-induced colon tumor growth and enhanced colon tumor apoptosis through epigenetics, oxidative, and signaling pathways.

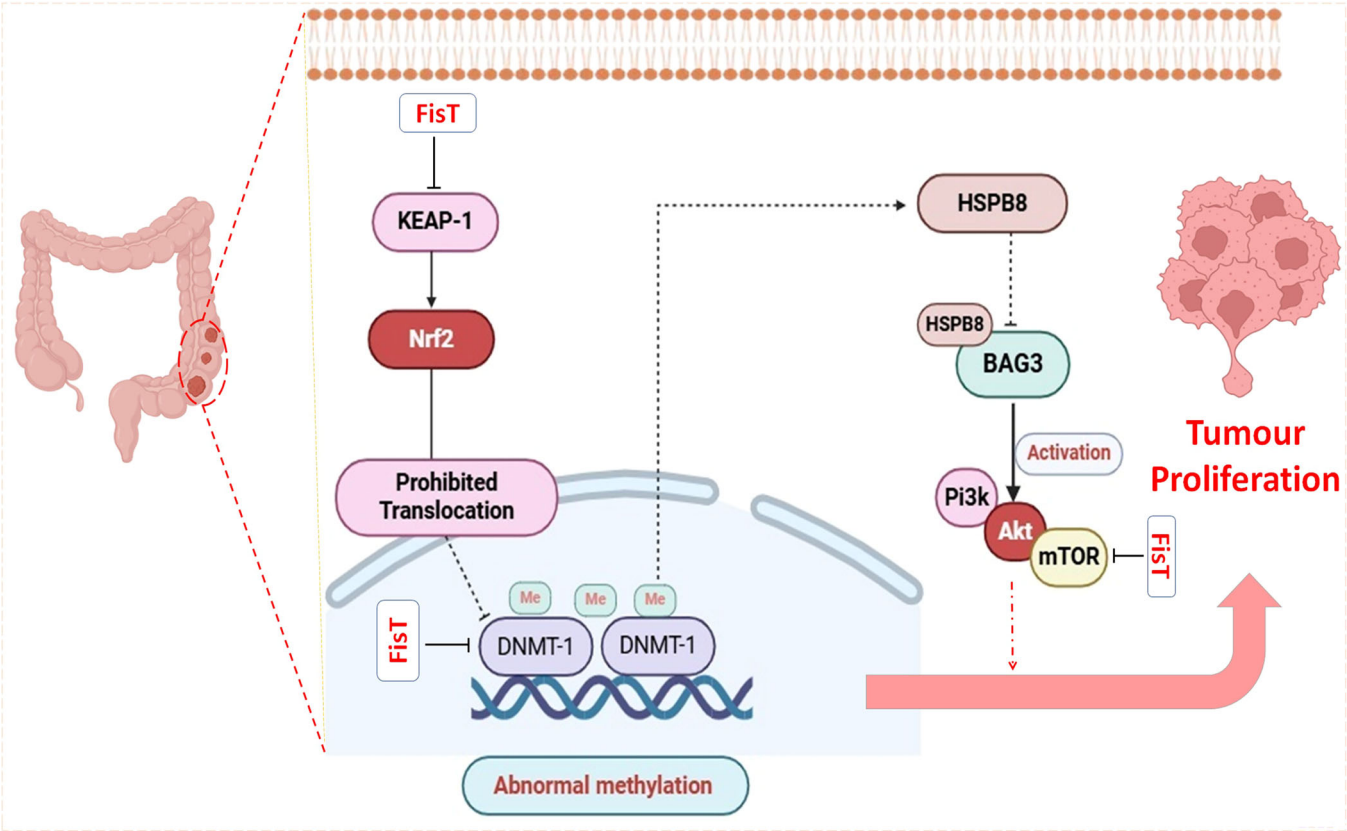

FIGURE 13 | The mechanistic insight of fisetin against the regulatory network of Keap-1/DNMT1 and mTOR axis in colon cancer.

5 | Conclusion

Utilizing a network pharmacology approach, FisT was found as the most active molecule, with mTOR, DNMT-1, and Keap-1 contributing as essential core proteins. Functional enrichment evaluation using KEGG pathways and GO keywords indicated that the mTOR, DNMT-1, and Keap-1 axis are critical for colon cancer development and metastasis. Molecular docking experiments verified the potential affinity of critical components for these hub genes with the favor of selected targets. Both in vitro and in vivo research showed that FisT could affect the hub genes on mTOR, DNMT-1, and Keap-1 via upregulation of the KEAP1 and downregulation of the DNMT1 and mTOR expression. Where previous findings only exploring the single target mostly by others Phyto molecules. Our study goes beyond the previous findings and explored these three pathways together which could be the best strategy to consider during therapeutic selection in patients. These findings support the accuracy and dependability of the pharmacological screening and mechanistic predictions investigated in this study, showing that FisT has the potential to improve lifespan and reduce cancer cell growth, tumor size, and metastasis. Further necessitate additional investigation to get more detailed mechanistic insights against colon cancer like enhancement of drug uptake by receptor-based internalization by using nanocarriers, drug peptide conjugates, and antibody drug conjugates followed by molecular profiling like proteomics, transcriptomic, and metabolomics to prove this hypothesis more strongly.

Acknowledgments

This work was supported by the Department of Pharmaceuticals, Ministry of Chemical and Fertilizers, Govt. of India. Authors are grateful to National Institute of pharmaceutical Education and Research, Hajipur and Ministry of pharmaceuticals, Government of India for technical and financial assistance in the terms of JRF and laboratory facilities.

Conflicts of Interest

The authors declare no conflicts of interest.

Data Availability Statement

Data would be made available on request.

References

1. M. P. Modarres, M. A. Habibi, M. R. Pashaei, Y. Mohammadpour, K. Jazi, and S. Ahmadpour, "Alterations of the Gut Microbiome and Metabolome Following: A Opportunity for Early Detection of Colorectal Cancer," *Current Cancer Therapy Reviews* 21, no. 1 (2025): 10–22.

2. R. Kong, N. Wang, W. Han, W. Bao, and J. Lu, "Fenofibrate Exerts Antitumor Effects in Colon Cancer via Regulation of DNMT1 and CDKN2A," *PPAR Research* 2021, no. 1 (2021): 6663782.

3. T. Wang, W. S. Zhang, Z. X. Wang, et al., "RAPTOR Promotes Colorectal Cancer Proliferation by Inducing mTORC1 and Upregulating Ribosome Assembly Factor URB1," *Cancer Medicine* 9, no. 4 (2020): 1529–1543.

4. A. Doostmohammadi, H. Jooya, K. Ghorbanian, S. Gohari, and M. Dadashpour, "Potentials and Future Perspectives of Multi-Target

Drugs in Cancer Treatment: The Next Generation Anti-Cancer Agents," *Cell Communication and Signaling: CCS* 22, no. 1 (2024): 228.

5. S. Cherri, E. Oneda, L. Zanotti, and A. Zaniboni, "Optimizing the First-Line Treatment for Metastatic Colorectal Cancer," *Frontiers in Oncology* 13 (2023): 1246716.

6. A. Esmeeta, S. Adhikary, V. Dharshnaa, et al., "Plant-Derived Bioactive Compounds in Colon Cancer Treatment: An Updated Review," *Biomedicine & Pharmacotherapy = Biomedecine & Pharmacotherapie* 153 (2022): 113384.

7. A. S. Adebayo, K. Agbaje, S. K. Adesina, and O. Olajubutu, "Colorectal Cancer: Disease Process, Current Treatment Options, and Future Perspectives," *Pharmaceutics* 15, no. 11 (2023): 2620.

8. M. M. Vuolo, V. S. Lima, and M. R. M. Junior, "Phenolic Compounds: Structure, Classification, and Antioxidant Power," in *Bioactive Compounds* (Elsevier, 2019), 33–50.

9. E. Amjad, B. Sokouti, and S. Asnaashari, "A Systematic Review of Anti-Cancer Roles and Mechanisms of Kaempferol as a Natural Compound," *Cancer Cell International* 22, no. 1 (2022): 260.

10. H. S. Tuli, V. K. Garg, S. Bhushan, et al., "Natural Flavonoids Exhibit Potent Anticancer Activity by Targeting Micrornas in Cancer: A Signature Step Hinting Towards Clinical Perfection," *Translational Oncology* 2023 27 (2023): 101596.

11. K. Demir, R. Turgut, S. Şentürk, H. Işıklar, and E. Günalan, "The Therapeutic Effects of Bioactive Compounds on Colorectal Cancer via PI3K/Akt/mTOR Signaling Pathway: A Critical Review," *Food Science & Nutrition* 12, no. 12 (2024): 9951–9973.

12. M. Y. Zamanian, N. Taheri, M. F. Ramadan, et al., "A Comprehensive View on the Fisetin Impact on Colorectal Cancer in Animal Models: Focusing on Cellular and Molecular Mechanisms," *Animal Models and Experimental Medicine* 7, no. 5 (2024): 591–605.

13. C. Zhou, Y. Huang, S. Nie, S. Zhou, X. Gao, and G. Chen, "Biological Effects and Mechanisms of Fisetin in Cancer: A Promising Anti-Cancer Agent," *European Journal of Medical Research* 28, no. 1 (2023): 297.

14. S. Somasundaram, M. E. Forrest, H. Moinova, et al., "The DNMT1-Associated lincRNA DACOR1 Reprograms Genome-Wide DNA Methylation in Colon Cancer," 2018, 10:1−15.

15. T. Aanniz, A. Bouyahya, A. Balahbib, et al., "Natural Bioactive Compounds Targeting DNA Methyltransferase Enzymes in Cancer: Mechanisms Insights and Efficiencies," *Chemico-Biological Interactions* 392 (2024): 110907.

16. G. Wang, "Identification and Verification of KEAP1-Related Genes and Targets Regulated by Potential Ingredients in KRAS Mutant Colorectal Cancer," 2024, 13(3): 148−166.

17. X.-J. Chi, "TBC1D10B Promotes Tumor Progression in Colon Cancer via PAK4-Mediated Promotion of the PI3K/AKT/mTOR Pathway," 2024: 1−13.

18. K. Demir, "The Therapeutic Effects of Bioactive Compounds on Colorectal Cancer via PI3K/Akt/mTOR Signaling Pathway: A Critical Review," 2024.

19. S. Hassani, H. Maghsoudi, F. Fattahi, et al., "Flavonoids Nanostructures Promising Therapeutic Efficiencies in Colorectal Cancer," *International Journal of Biological Macromolecules* 241 (2023): 124508.

20. X. Chen, C. Shi, M. He, S. Xiong, and X. Xia, "Endoplasmic Reticulum Stress: Molecular Mechanism and Therapeutic Targets," *Signal Transduction and Targeted Therapy* 8, no. 1 (2023): 352.

21. M. Hu, L. Yuan, and J. Zhu, "The Dual Role of NRF2 in Colorectal Cancer: Targeting NRF2 as a Potential Therapeutic Approach," *Journal of Inflammation Research* 17 (2024): 5985–6004.

22. S. Zhang, S. Duan, Z. Xie, et al., "Epigenetic Therapeutics Targeting NRF2/KEAP1 Signaling in Cancer Oxidative Stress," *Frontiers in Pharmacology* 13 (2022): 924817.

23. F. Pouremamali, A. Pouremamali, M. Dadashpour, N. Soozangar, and F. Jeddi, "An Update of Nrf2 Activators and Inhibitors in Cancer Prevention/Promotion," *Cell Communication and Signaling: CCS* 20, no. 1 (2022): 100.

24. P. Peng, "Epigenetic Remodeling Under Oxidative Stress: Mechanisms Driving Tumor Metastasis," 2024, 3 (4): e70000.

25. B. Buranrat, "Fisetin-Induced Cell Death, Apoptosis, and Anti-migratory Effects in Cholangiocarcinoma Cells," 2025, 15(2): 096−105.

26. R. Ma, X. Liu, P. Zheng, G. Zou, and C. Zhang, "Tectorigenin Alleviates Irinotecan-Induced Intestinal Inflammation by Activating the Nrf2/Keap1 Pathway and Synergistically Enhances the Anti-Colon Cancer Efficacy of Irinotecan," *Toxicology and Applied Pharmacology* 502 (2025): 117416.

27. H. Dong and C. Zhang, "Epigenetic and Biogenetic Regulation by Polyphenols in Prostate Cancer in the Context of 3P Medicine," *EPMA Journal* 16, no. 1 (2025): 113–125.

28. P. Garg, S. Ramisetty, M. Nair, et al., "Strategic Advancements in Targeting the PI3K/AKT/mTOR Pathway for Breast Cancer Therapy," *Biochemical Pharmacology* 236 (2025): 116850.

29. X. Qian, Q. Y. Bi, Z. N. Wang, et al., "Qingyihuaji Formula Promotes Apoptosis and Autophagy Through Inhibition of MAPK/ERK and PI3K/Akt/mTOR Signaling Pathway on Pancreatic Cancer In Vivo and In Vitro," *Journal of Ethnopharmacology* 307 (2023): 116198.

30. U. Desai, "Modulation of Drug Resistance in Leukemia Using Phytochemicals: An In-Silico, In-Vitro, and In-Vivo Approach," in *Recent Frontiers of Phytochemicals* (Elsevier, 2023), 583–599.

31. A. Syriopoulou, I. Markopoulos, A. G. Tzakos, and T. Mavromoustakos, "Ligand–Receptor Interactions and Drug Design," *Methods in Molecular Biology (Clifton, N.J.)* 2266 (2021): 89–104.

32. H. Luthufi and H. Mudalige, "Protein-Ligand Docking to Identify Potential Phytochemicals Against Breast Cancer Protein Receptor Using Autodock," 2022.

33. S. Poblete, S. Pantano, K. Okazaki, Z. Liang, K. Kremer, and A. B. Poma, "Editorial: Recent Advances in Computational Modelling of Biomolecular Complexes," *Frontiers in Chemistry* 11 (2023): 1200409.

34. C. Yaacoub, M. Rifi, D. El-Obeid, et al., "The Cytotoxic Effect of *Apis mellifera* Venom With a Synergistic Potential of Its Two Main Components—Melittin and PLA2—On Colon Cancer HCT116 Cell Lines," *Molecules* 26, no. 8 (2021): 2264.

35. C. Zhou, M. Wang, X. Du, et al., "WTAP/IGF2BP3 Mediated m6A Modification of SOD2 mRNA Aggravates the Tumourigenesis of Colorectal Cancer," *Journal of Biochemical and Molecular Toxicology* 39, no. 1 (2025): 70117.

36. A. Aslam, "Folic Acid-Grafted Poly-3-Hydroxybutyrate Nanoparticles for Enhanced pH-Sensitive Paclitaxel Delivery and Cancer Cell Targeting," 2025: 136141.

37. N. Nishizawa, R. Arai, K. Hiranuma, M. Toya, and M. Sato, "CAMSAP2 Is Required for Bridging Fiber Assembly to Ensure Mitotic Spindle Assembly and Chromosome Segregation in Human Epithelial Caco-2 Cells," *PLoS One* 20, no. 1 (2025): e0308150.

38. O. G. Lyublinskaya, J. S. Ivanova, N. A. Pugovkina, et al., "Redox Environment in Stem and Differentiated Cells: A Quantitative Approach," *Redox Biology* 12 (2017): 758–769.

39. L. J. Bou Malhab, "Exploring the Anticancer Effect of *Artemisia herba-alba* on Colorectal Cancer: Insights From Eight Colorectal Cancer Cell Lines," 2025, 13(1): e4715.

40. Y. E. Jeong, K. Shea, and K. A. Ford, "Unraveling Caco-2 Cells Through Functional and Transcriptomic Assessments," *Regulatory Toxicology and Pharmacology: RTP* 156 (2025): 105771.

41. Y. Abdollahzadeh, M. Mazandarani, S. H. Hoseinifar, T. Lieke, H. Van Doan, and S. Pourmozaffar, "Dietary Fulvic Acid Improves

Immune, Digestive and Antioxidant Parameters in Juvenile White-Leg Shrimp (*Litopenaeus vannamei*) in a Super-Intensive System," *Comparative Biochemistry and Physiology. Part B, Biochemistry & Molecular Biology* 275 (2025): 111011.

42. Y. Xuan, W. Yan, R. Wang, et al., "GM-CSF and IL-21-Armed Oncolytic Vaccinia Virus Significantly Enhances Anti-Tumor Activity and Synergizes With Anti-PD1 Immunotherapy in Pancreatic Cancer," *Frontiers in Immunology* 15 (2024): 1506632.

43. Y. Wang, Y. Chen, H. Zhang, S. Yu, G. Yuan, and H. Hu, "Colon-Targeted Self-Assembled Nanoparticles Loaded With Berberine Double Salt Ameliorate Ulcerative Colitis by Improving Intestinal Mucosal Barrier and Gut Microbiota," *Colloids and Surfaces, B: Biointerfaces* 245 (2025): 114353.

44. G. Yuan, "LPS-Induced Extracellular AREG Triggers Macrophages Pyroptosis Through EGFR/TLR4 Signaling Pathway," 2025.

45. L. Kovács and D. András, "Tumor Volume Measurements in Animal Experiments: Current Approaches and Their Limitations." 2023.

46. M. Kowalczyk, M. Orłowski, Ł. Klepacki, et al., "Rectal Aberrant Crypt Foci (ACF) as a Predictor of Benign and Malignant Neoplastic Lesions in the Large Intestine," *BMC Cancer* 20 (2020): 133.

47. X. He, G. Li, L. Huang, et al., "Nonviral Targeted mRNA Delivery: Principles, Progresses, and Challenges," *MedComm* 6, no. 1 (2025): 70035.

48. Z. Huang, L. Liao, Z. Wang, et al., "An Efficient Approach for Wholemount Preparation of the Myenteric Plexus of Rat Colon," *Journal of Neuroscience Methods* 348 (2021): 109012.

49. M. Bistoletti, G. Micheloni, N. Baranzini, et al., "Homeoprotein OTX1 and OTX2 Involvement in Rat Myenteric Neuron Adaptation After DNBS-Induced Colitis," *PeerJ* 8 (2020): 8442.

50. M. Russo, S. Moccia, D. Luongo, and G. L. Russo, "Senolytic Flavonoids Enhance Type-I and Type-II Cell Death in Human Radioresistant Colon Cancer Cells Through AMPK/MAPK Pathway," *Cancers* 15, no. 9 (2023): 2660.

51. A. Pandey and S. K. Trigun, "Fisetin Induces Apoptosis in Colorectal Cancer Cells by Suppressing Autophagy and Down-Regulating Nuclear Factor Erythroid 2-Related Factor 2 (Nrf2)," *Journal of Cellular Biochemistry* 124, no. 9 (2023): 1289–1308.

52. V. Barra, R. F. Chiavetta, S. Titoli, I. M. Provenzano, P. S. Carollo, and A. Di Leonardo, "Specific Irreversible Cell-Cycle Arrest and Depletion of Cancer Cells Obtained by Combining Curcumin and the Flavonoids Quercetin and Fisetin," *Genes* 13, no. 7 (2022): 1125.

53. Rd. P. do Nascimento, "The Preventive and Therapeutic Potential of Native Brazilian Fruits on Colorectal Cancer," 2022, 46: 101539.

54. H. Xiao, X. Hao, B. Simi, et al., "Green Tea Polyphenols Inhibit Colorectal Aberrant Crypt Foci (ACF) Formation and Prevent Oncogenic Changes in Dysplastic ACF in Azoxymethane-Treated F344 Rats," *Carcinogenesis* 29, no. 1 (2008): 113–119.

55. B. D. Sahu, J. M. Kumar, and R. Sistla, "Fisetin, a Dietary Flavonoid, Ameliorates Experimental Colitis in Mice: Relevance of NF-κB Signaling," *Journal of Nutritional Biochemistry* 28 (2016): 171–182.

56. A. Farsad-Naeimi, M. Alizadeh, A. Esfahani, and E. Darvish Aminabad, "Effect of Fisetin Supplementation on Inflammatory Factors and Matrix Metalloproteinase Enzymes in Colorectal Cancer Patients," *Food & Function* 9, no. 4 (2018): 2025–2031.

57. Y. Cai, E. J. Geutjes, K. de Lint, et al., "The NuRD Complex Cooperates With DNMTs to Maintain Silencing of Key Colorectal Tumor Suppressor Genes," *Oncogene* 33, no. 17 (2014): 2157–2168.

58. A. A. Farooqi, H. Naureen, R. Zahid, L. Youssef, R. Attar, and B. Xu, "Cancer Chemopreventive Role of Fisetin: Regulation of Cell Signaling Pathways in Different Cancers," *Pharmacological Research* 172 (2021): 105784.

59. Y. Chen, D. Jiao, H. He, et al., "Disruption of the Keap1-mTORC2 Axis by Cancer-Derived Keap1/mLST8 Mutations Leads to Oncogenic mTORC2-AKT Activation," *Redox Biology* 67 (2023): 102872.

60. C. Chen, Z. Wang, Y. Ding, et al., "DNA Methylation: From Cancer Biology to Clinical Perspectives," *Frontiers in Bioscience-Landmark* 27, no. 12 (2022): 326.

61. L. Yan, Q. Geng, Z. Cao, et al., "Insights into DNMT1 and Programmed Cell Death in Diseases," *Biomedicine & Pharmacotherapy* 168 (2023): 115753.

62. J. Wang, L. Xu, X. Liu, R. Yang, and D. Wang, "A Facile Adenosine Triphosphate-Responsive Nanoplatform for Efficacious Therapy of Esophageal Cancer," *Oncology Letters* 20, no. 4 (2020): 1.

63. O. Ramos-Lopez, F. I. Milagro, J. I. Riezu-Boj, and J. A. Martinez, "Epigenetic Signatures Underlying Inflammation: An Interplay of Nutrition, Physical Activity, Metabolic Diseases, and Environmental Factors for Personalized Nutrition," *Inflammation Research* 70 (2021): 29–49.

64. T. Setiawan, I. N. Sari, Y. T. Wijaya, et al., "Cancer Cachexia: Molecular Mechanisms and Treatment Strategies," *Journal of Hematology & Oncology* 16, no. 1 (2023): 54.

65. P.-J. Tsai, Y. H. Lai, R. K. Manne, Y. S. Tsai, D. Sarbassov, and H. K. Lin, "Akt: A Key Transducer in Cancer," *Journal of Biomedical Science* 29, no. 1 (2022): 76.

66. Z. Koveitypour, F. Panahi, M. Vakilian, et al., "Signaling Pathways Involved in Colorectal Cancer Progression," *Cell & Bioscience* 9, no. 1 (2019): 97.

67. P. H. Hoang and M. T. Landi, "DNA Methylation in Lung Cancer: Mechanisms and Associations With Histological Subtypes, Molecular Alterations, and Major Epidemiological Factors," *Cancers* 14, no. 4 (2022): 961.

68. F. Yang, X. Liu, Y. Li, et al., "Evolutionary Analysis of the mTOR Pathway Provide Insights Into Lifespan Extension Across Mammals," *BMC Genomics* 24, no. 1 (2023): 456.

69. T. V. Saco, M. T. Breitzig, R. F. Lockey, and N. Kolliputi, "Epigenetics of Mucus Hypersecretion in Chronic Respiratory Diseases," *American Journal of Respiratory Cell and Molecular Biology* 58, no. 3 (2018): 299–309.

70. R. Ahmad, "Emerging Trends in Colorectal Cancer: Dysregulated Signaling Pathways," 2021, 47(3): 14.

71. Z.-N. Lei, Q. X. Teng, Q. Tian, et al., "Signaling Pathways and Therapeutic Interventions in Gastric Cancer," *Signal Transduction and Targeted Therapy* 7, no. 1 (2022): 358.